CRYOGENIC REFRIGERATION USING AN ACOUSTIC STIRLING EXPANDER

Masters Thesis by Nick Emery
Department of Mechanical Engineering, University of Canterbury
Christchurch, New Zealand

Abstract

A single-stage pulse tube cryocooler was designed and fabricated to provide cooling at 50 K for a high temperature superconducting (HTS) magnet, with a nominal electrical input frequency of 50 Hz and a maximum mean helium working gas pressure of 2.5 MPa. Sage software was used for the thermodynamic design of the pulse tube, with an initially predicted 30 W of cooling power at 50 K, and an input indicated power of 1800 W. Sage was found to be a useful tool for the design, and although not perfect, some correlation was established. The fabricated pulse tube was closely coupled to a metallic diaphragm pressure wave generator (PWG) with a 60 ml swept volume. The pulse tube achieved a lowest no-load temperature of 55 K and provided 46 W of cooling power at 77 K with a p-V input power of 675 W, which corresponded to 19.5% of Carnot COP. Recommendations included achieving the specified displacement from the PWG under the higher gas pressures, design and development of a more practical co-axial pulse tube and a multi-stage configuration to achieve the power at lower temperatures required by HTS.

Acknowledgements

The author acknowledges: His employer, Industrial Research Ltd (IRL), New Zealand, for the continued support of this work, Alan Caughley for all his encouragement, help and guidance, New Zealand's Foundation for Research, Science and Technology for funding, University of Canterbury – in particular Alan Tucker and Michael Gschwendtner for their excellent supervision and helpful input, David Gedeon for his Sage software and great support, Mace Engineering for their manufacturing assistance, my wife Robyn for her support, and HTS-110 for creating an opportunity and pathway for the commercialisation of the device.

Table of Contents

List of Figures

List of Tables

1 Introduction

Industrial Research Ltd (IRL) began research in cryogenic refrigeration in 2004 with a project objective of creating an industrialised cryocooler for cooling High Temperature Superconducting (HTS) applications such as transformers and magnets. IRL's initial work in the cryogenic refrigeration programme concentrated on the compressor side of the refrigerator. This led to a novel pressure wave generator (PWG) technology using metallic diaphragms[1,2] to separate the clean cryocooler working gas from a conventionally lubricated driving mechanism. The first 200 ml swept volume PWGs successfully powered a number of pulse tube refrigerators (PTR)[1,2]. IRL made a pulse tube for a 20 ml swept volume PWG that achieved 7 W of refrigeration at 77 K[2].

This thesis describes the design, manufacture and experimental optimization of a PTR. Outside the scope of this project, a 60 ml PWG has been designed in-house for the purpose of powering the pulse tube. The planned outcome is to produce a PTR capable of cooling an HTS magnet manufactured by HTS-110 Ltd. The cooling requirement for the magnet is 20 W @ 50 K, hence this pulse tube was designated the PT2050. Knowledge in the modelling, design, manufacture, assembly and tuning of pulse tubes, in combination with PWG design, will be useful for subsequent refrigerators.

1.1 Overview

The first reported use of the term cryogenic was in 1894 by Dr. H. Kammerlingh Onnes on the cryogenic laboratory at Leiden and on the production of very low temperatures[4]. A Cryocooler is a refrigerator that removes heat at cryogenic temperatures (typically below 120 K) and rejects the heat at ambient temperature. Table 1.1 shows some of the common temperature scales, and highlights the fact that 0 K is equivalent to -273 °C, so these coolers generally operate below -150 °C.

Table 1.1. Common temperature scales

Kelvin (K)	Celsius (°C)	Fahrenheit (°F)
0	-273.15	-459.67
273.15	0	32
373.15	100	212

Several cryocooler concepts exist. Mostly these can be divided into regenerative and recuperative cycles, as shown in Table 1.2, based on the type of flow required to run the system. Recuperative cycles have a steady flow of gas circulating between the warm and cold parts of the cooler. A counter-flow heat exchanger (recuperator) is used to cool the warm stream and warm the cold stream. Regenerative cycles oscillate the same gas between warm and cold regions, transferring energy to and from a solid matrix (a regenerator), as the gas moves between temperature regions.

Table 1.2. Common cycles and heat exchanger types

Cycle	Heat Exchanger
Stirling	Regenerative
Pulse tube	Regenerative
Gifford-McMahon (GM)	Regenerative
Brayton	Recuperative
Joule-Thomson (JT)	Recuperative
Claude	Recuperative

This thesis concerns the development of a pulse tube: Pulse tubes can be run at a number of different frequencies depending on their design. They generally fall into either a low frequency (approximately 1 Hz) or high frequency (30+ Hz) category. A Gifford-McMahon system can power a low frequency pulse tube. This system uses a gas tank system with valves to allow gas to pass back and forth through the pulse tube. The lower frequency systems can generally cool to lower temperatures but suffer from poorer power density.

Several applications exist for pulse tube cryocoolers such as:

- Gas liquefiers for gases such as oxygen, CO_2, and helium
- Medical applications such as cryosurgery
- Cooling of superconducting magnets for applications such as MRI scanners in the medical industry
- Sensor cooling in space and military applications
- Cryo-pumping for achieving high vacuums in the semi-conductor industry

Figure 1.1 shows the temperature and cooling power capabilities of available technologies and overlays with the temperature and cooling requirements of various applications that operate at cryogenic temperatures. The pulse tube areas are shown in yellow and are split into high and low frequency.

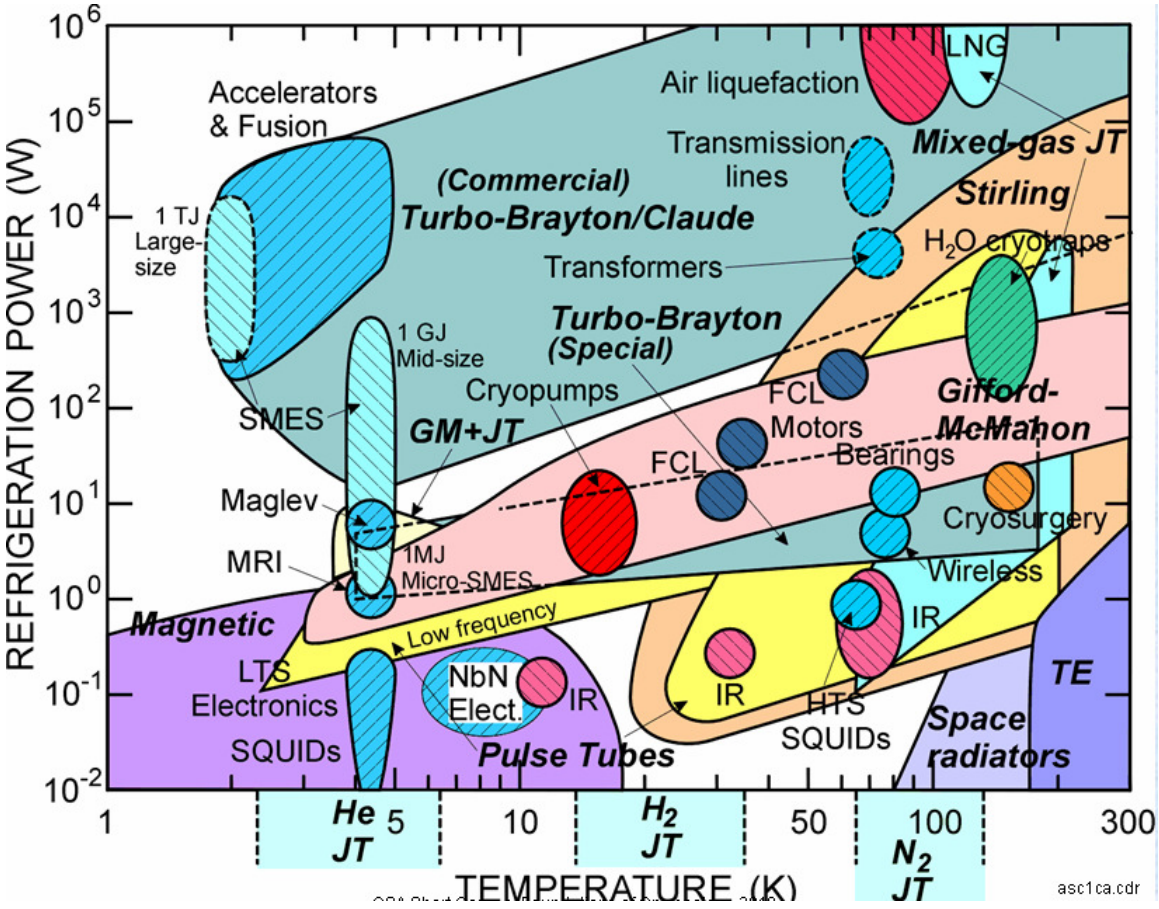

Figure 1.1. Landscape of cooler types (bold typeface) and applications (source: Radebaugh[3])

1.2 Background

The pulse tube is a variant of the Stirling cycle. The Stirling cycle was invented by the Scottish Church Minister Robert Stirling, with the help of his brother who was an engineer, in 1817. This preceded the Carnot Cycle, which was first discussed in the book "Reflections on the Motive Power of Fire[4]" in the year 1824 by the young French scientist Sadi Carnot. The first Stirling machine was an engine, which was conceived to rival the steam engine as a prime mover. It was later discovered that the cycle could be reversed to provide refrigeration. This thesis will be concerned only with the reversed cycle, which is also called a heat pump.

Robert Stirling also invented a very important component, which he called the "economizer". This has later come to be known as the regenerator, which was the term used by Ericsson for his independent invention of the mixed-flow counter-current heat exchanger, which came after Stirling's invention. This component allows heat energy to be stored in a porous medium as the gas flows from the hot to the cold part of the cycle. The stored energy is returned to the gas when it passes back through the regenerator, since the flow oscillates.

The pulse tube is a refrigerator, as opposed to a heat engine that operates in direct mode. It uses a section of gas enclosed in a tube, which is subjected to pressure fluctuations at one end, causing an effect comparable with that of a mechanical expander piston in the Stirling cycle. The Stirling and the Ericsson cycles are regenerative processes, which both assume isothermal compression and expansion processes. The two ideal cycles differ in that the Stirling (Figure 1.2) includes isochoric heat addition and removal, where the Ericsson uses two isobaric heat processes. Both of these ideal cycles do not take into account the fact that the gas is oscillating and that a particle of gas does not pass through the entire cycle. A GM machine is comparable to the Ericsson cycle, where a high frequency pulse tube could be compared to the Stirling cycle. The higher the frequency of operation the closer the compression and expansion processes get to the adiabatic case.

The lower the frequency, and the more surface area and cooling available, the closer to isothermal the processes become.

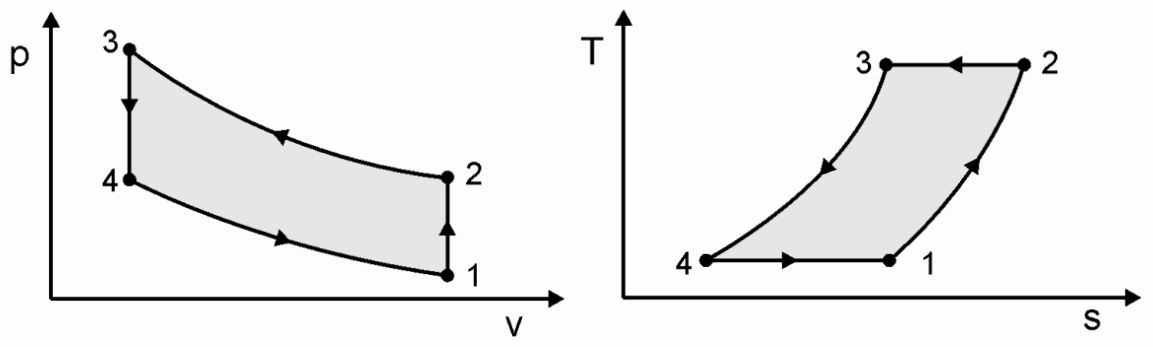

Figure 1.2. Stirling cycle p-V and T-s diagrams

The idealised Reversed Stirling cycle pressure-volume (p-V) and temperature-entropy (T-s) diagrams are shown in Figure 1.2. The four thermodynamic processes are described:

1 – 2 **Isochoric heat-addition.** The gas passes back through the regenerator where it recovers much of the heat transferred in 4 – 1, heating up on its way to the compression space.

2 – 3 **Isothermal Compression.** The compression space and associated heat exchanger are maintained at ambient temperature so the gas undergoes isothermal compression rejecting heat to the ambient sink.

3 – 4 **Isochoric heat-removal**. The gas is passed through the regenerator, where it cools transferring heat to the regenerator for use in the next cycle.

4 – 1 **Isothermal Expansion**. The expansion-space and associated heat exchanger are maintained at a constant low temperature, and the gas undergoes isothermal expansion absorbing heat at the cold sink.

The area enclosed by the p-V diagram is the work done, and is therefore called the p-V work or input power. The area enclosed by the T-s diagram is the amount of thermal energy required to drive the ideal cycle.

There is a variety of ways in which the Stirling cycle concept can be embodied in real machines, which attempt to mimic – but inevitably deviate from – the sequence of processes that make up the ideal cycle. Depending on the mechanical layout, Stirling machines can be classified as being Alpha, Beta or Gamma configuration. The schematic representation in Figure 1.3 is a comparison between the Gamma configuration Stirling refrigerator and a pulse tube refrigerator. The Beta and Gamma Stirling machines use a separate displacer piston, which means that the driving piston does both the compression and expansion work. The Alpha type reversed Stirling uses an expander piston mechanically driven to aid cooling, and could be used to better represent the pulse tube.

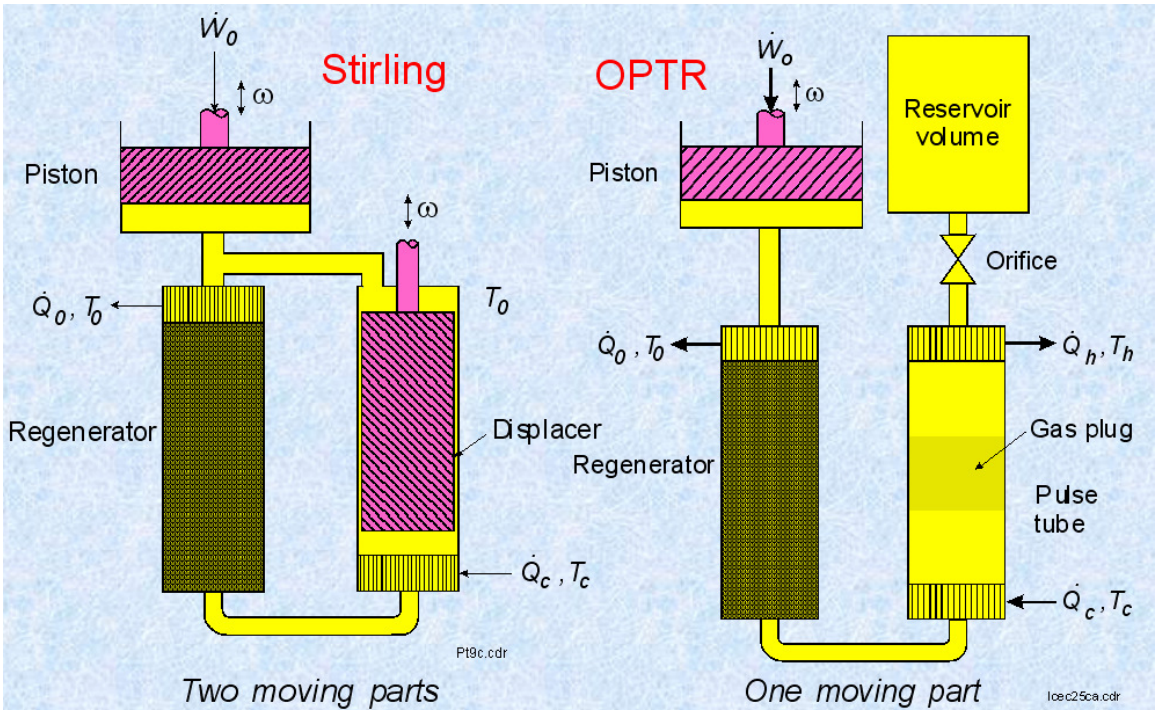

Figure 1.3. Comparison between the Gamma Stirling and a pulse tube cooler (source: Radebaugh[3])

An advantage of the pulse tube is that there are no moving parts with associated wearing components in the cold region. A mechanism for providing a phase shift (about 90°) between the gas mass flow in the pulse tube expansion space and the mass flow in the compression space, whilst minimizing losses associated with the phase shift, is required for a pulse tube to operate most efficiently.

2 Pulse Tube History

2.1 Early Developments

The first pulse tube[5] was discovered in the early 1960's when Professor William Gifford and a student Ralph Longsworth noticed that a pipe on their low frequency Gifford-McMahon system was getting cold at one end and was warm at the other end.

Three of the common pulse tube configurations are shown in Figure 2.1. The inline system is the easiest to manufacture since the flow in the U-tube and Co-axial systems have to perform a 180° change in direction at the cold-head. Conversely the inline system is the least practical since the cold-head is placed between two warm heat exchangers. All three configurations are shown with an orifice valve and reservoir phase shifter.

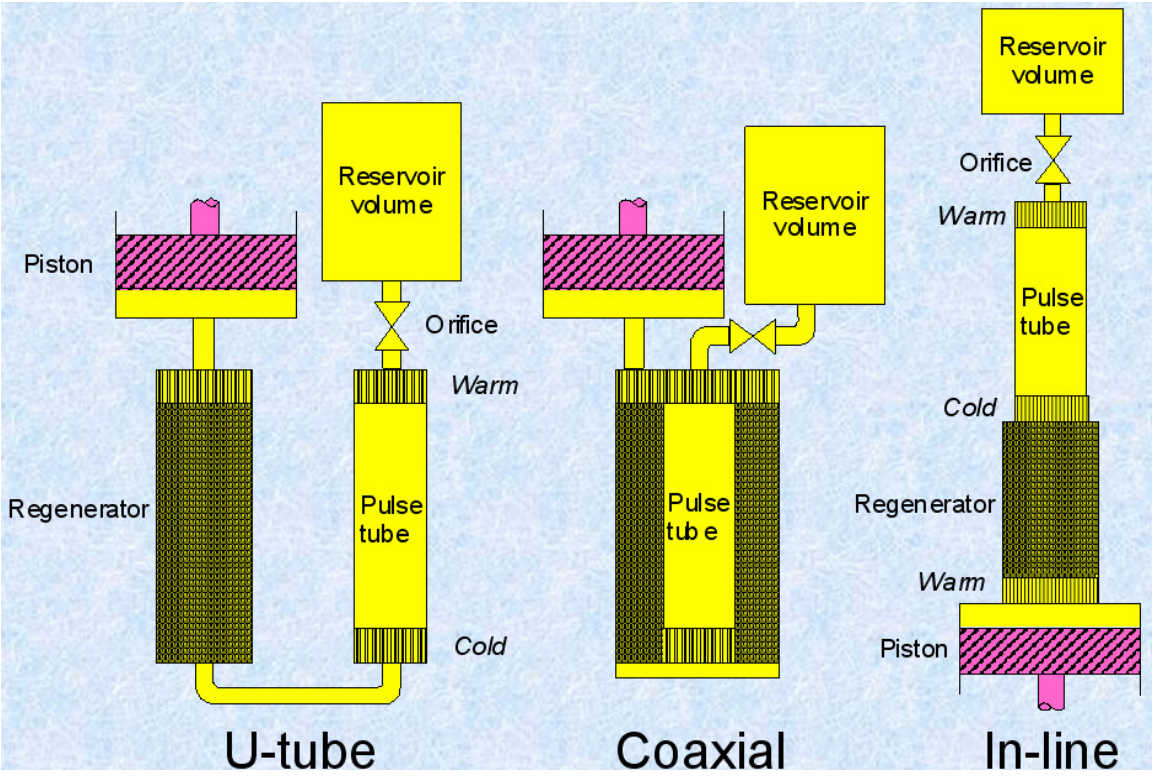

Figure 2.1. Examples of different pulse tube configurations

(source: Radebaugh[3])

A history of some of the more significant developments of the pulse tube is shown in Table 2.1.

Table 2.1. A brief history of some significant pulse tube developments

Development	Year	Author
First Pulse tube	1963	Gifford et al.[5]
Orifice and Reservoir	1984	Mikulin et al.[6]
Moving plug/hot piston	1988	Matsubara et al.[7]
Double inlet	1990	Zhu et al.[8]
Multiple by-pass	1992	Yang et al.[9]
Inertance tube	1994	Kanau et al.[10]
DC flow suppressor on double inlet	2007	Hu et al.[11]

After Gifford and Longsworth's discovery they developed a concept, which achieved a lowest temperature of 190 K. 20 years later in 1984 Mikulin et al. added an orifice valve restriction and reservoir volume to create a phase shift between the mass flow rate of the gas and the pressure oscillation, by way of a resistance to the mass flow. A more efficient phase shifter, the inertance tube, was first used in 1994 by Kanau et al., which used resonance to create the phase shift; a lowest temperature of 98 K was achieved. The inertance tube and reservoir phase shifter will be discussed in more detail in later chapters. The pulse tube refrigerator that this thesis is based on uses an inertance tube for phase shifting.

Matsubara et al. described a moving plug pulse tube in 1988, which allows the expansion work to be recovered by an active device.

3D streaming losses were found to be occurring in the regenerator, created by a large mass-flow that reduced the pressure ratio available for expansion work; this problem was solved in part by the double inlet valve (Figure 2.2), which was first used in 1990 by Zhu et al. A circulating DC flow was found to occur with the double inlet valve, and a means

of overcoming this was described by Hu in 2007. The DC flow suppressor for the double inlet PTR does as the name suggests, only allow an AC flow, which thereby prevents the power-consuming circulating mass flow.

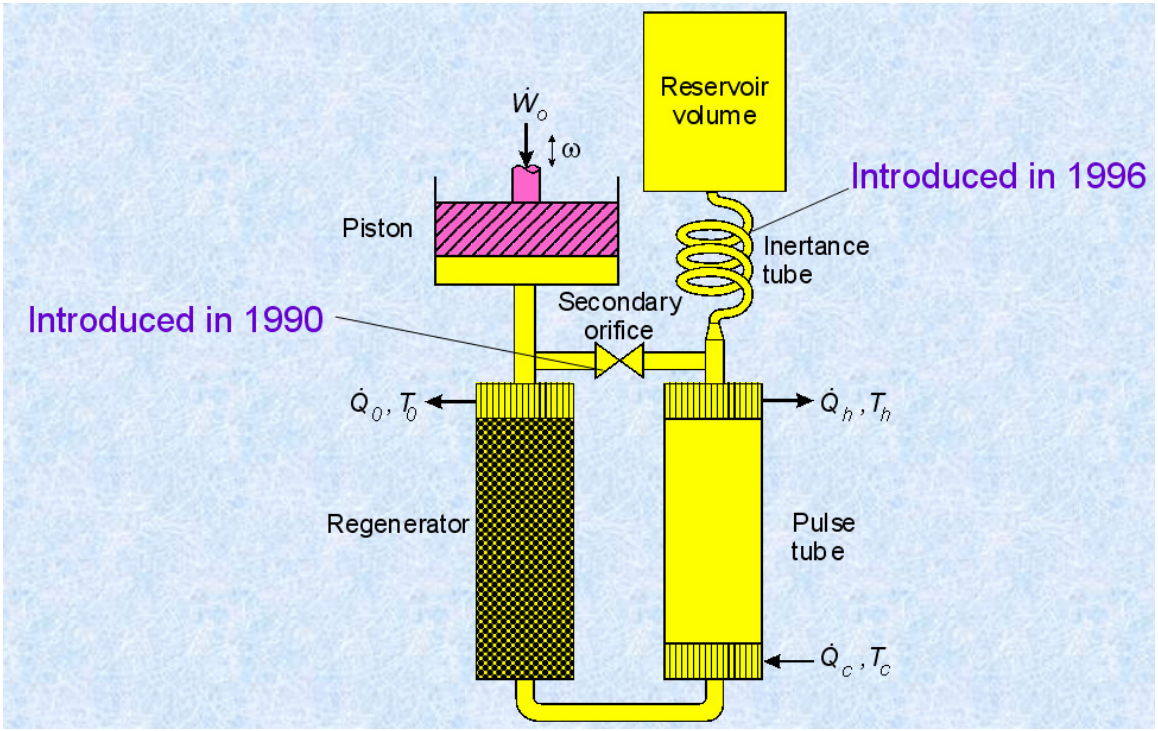

Figure 2.2. Double inlet and inertance tube pulse tube refrigerator (source: Radebaugh[3])

2.2 Recent Advances

Combined cycle systems, multi-staging, magnetic additions, materials research and 3D thermal and flow effects are just a few of the areas of interest to the cryocooler community. Driving frequencies greater than 100 Hz to improve power density, and low temperatures down into the milli-Kelvin range are some of the research areas currently being explored to push the boundaries. The usual requirements asked of any piece of machinery such as reduced weight, less vibration, lower cost and higher efficiency are high on the agenda of many research groups around the world.

3 Pulse Tube Theory

3.1 Phase Relationships

The pulse tube theory is not fully understood yet. Unfortunately there is not an ideal "Pulse tube Cycle" to compare the pulse tube to. An attempt will be made in this chapter to try and identify significant areas of interest in the analysis of the pulse tube refrigerator.

The pulse tube system requires a PWG to provide the compression and expansion work, with the pressure wave forcing the gas back and forth through a series of components in an enclosed and pressurized environment. The basic principle is that when a finite mass of gas is compressed (work is done on it) the temperature of the gas increases, and when a finite mass of gas is expanded its temperature decreases. By removing heat from the process a net steady state cooling is achieved. While this explanation makes the concept appear to be simple, the practical implementation is somewhat more complicated.

The pressure wave degrades in terms of amplitude the further away from the compression piston it is measured. This is due to dissipative effects such as pressure drops and heat losses/gains, and compression of the gas through the system. There is also an associated phase shift between the mass flow and the pressure wave. This phase shift occurs because the gas has a mass and a spring-rate, and also a pressure drop that corresponds to damping (frictional losses), where the pressure wave travels at the speed of sound through the system. The virtual expander piston, which the pulse tube effectively represents, requires a phase shift to allow the gas to expand at the appropriate time.

One main difference between a Gamma Stirling machine and a pulse tube is that the gamma Stirling displacer piston leads its compression piston in terms of mechanical phasing, where the pulse tube virtual expansion piston lags behind its compression piston. A comparison between the ideal Stirling cycle and a real pulse tube is usually carried out by measuring the compression piston pressure and displacement.

3.1.1 Phasor Diagrams

The pressure and flow are complex quantities in the oscillating flow of a pulse tube, and therefore the real and imaginary components can be represented by vectors on a plane. Phasor diagrams are a graphical representation of the pressure and flow phase angle, with a real and an imaginary axis. The Phasor diagrams shown in Figures 3.2 and 3.3 have been based on the ideal gas law.

Figure 3.2 shows the pressure–flow phase through an orifice pulse tube cooler. The schematic shows that the phase of the mass flow rate of gas with respect to the pressure is zero at the warm end of the pulse tube, by the orifice valve. This is because of the inefficient resistive nature of the orifice valve.

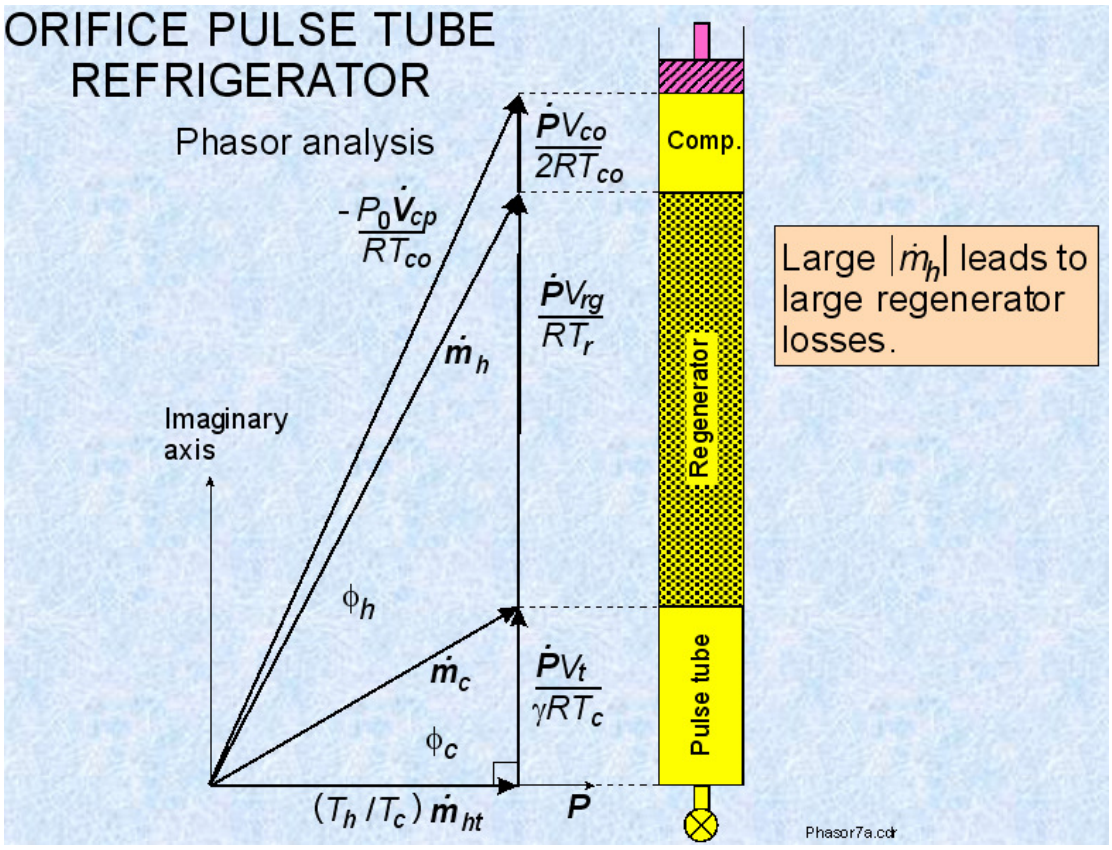

Figure 3.2. Phasor analysis of an orifice pulse tube cooler

(source: Radebaugh[3])

The gas phasor analysis for an inertance tube phase shifted pulse tube is shown in Figure 3.3. Compared to the orifice phase shifter it is possible to obtain zero mass flow rate phase to the pressure oscillation at the centre of the regenerator, which minimises flow losses since pressure drop and non-ideal heat transfer are quite dependent on the mass flow rate through the regenerator[3]. The inertance tube phase shifter makes this possible due to its resonant, rather than purely resistive, phase shifting qualities, which are described on more detail in Section 3.3.

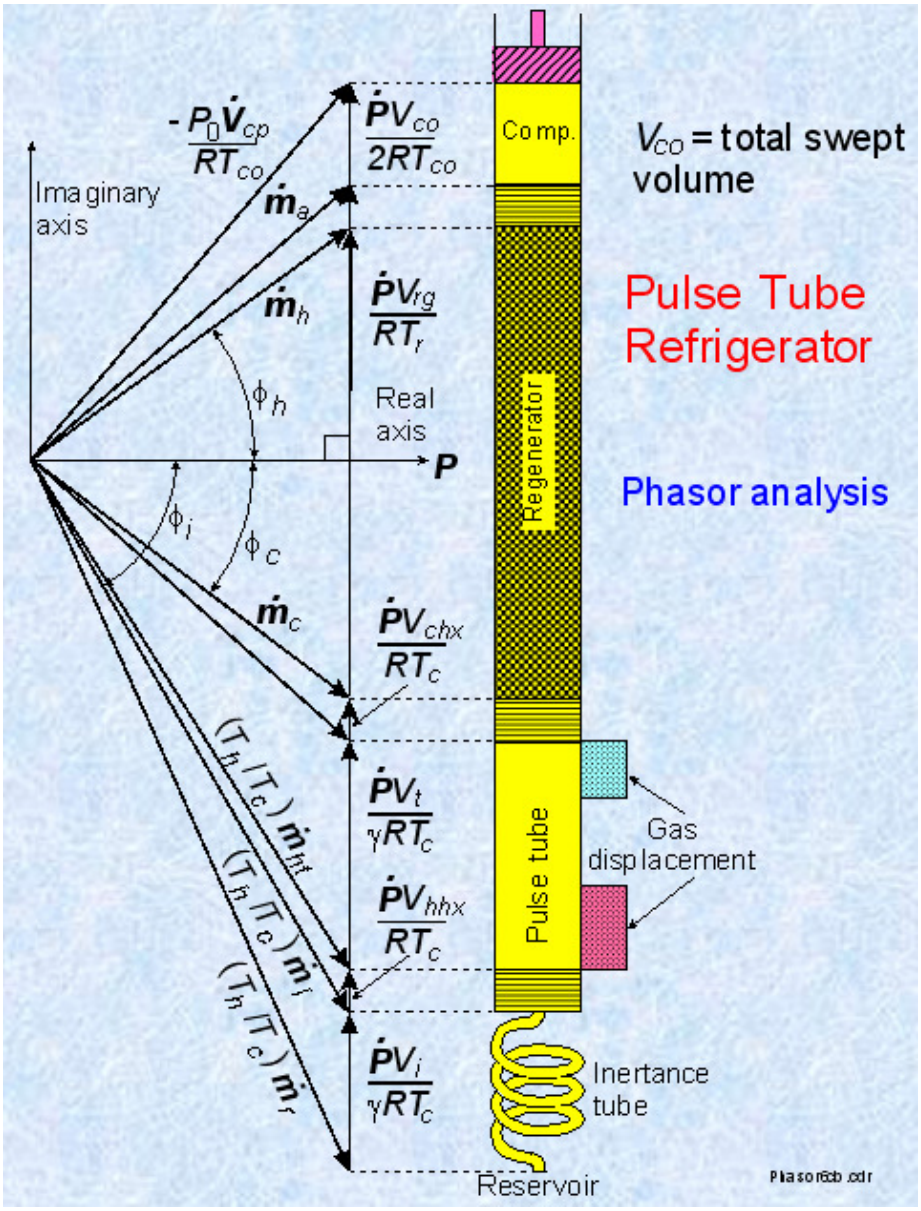

Figure 3.3. Phasor analysis of an inertance tube pulse tube refrigerator (source: Radebaugh[3])

3.2 Cycle Coefficient of Performance

The modelling of the characteristics of the pulse tube cooler was carried out to gain an understanding of the fundamental principles, as well as to help verify further more complex models of the system. The Coefficient of Performance (COP) of the orifice pulse tube is defined as[3]:

$$COP_{PT} = \frac{T_C}{T_0} \qquad \text{Eq (3.3.1)}$$

With a cold temperature of 50 K and an ambient rejection temperature of 300 K the calculated COP of the orifice pulse tube, using Equation 3.3.1, is 17 %. The Carnot efficiency is defined as:

$$COP_{CARNOT} = \frac{T_C}{T_0 - T_C} \qquad \text{Eq (3.3.2)}$$

Using the same values as for the orifice pulse tube COP (50 K and 300 K), Equation 3.3.2 gives a Carnot COP of 20 %. A more meaningful COP in common use is the percentage of Carnot COP of the pulse tube (i.e. how good is it compared to the ideal case – so it is therefore termed the Carnot efficiency):

$$\eta_{CARNOT} = \frac{COP_{PT}}{COP_{CARNOT}} \qquad \text{Eq (3.3.3)}$$

Applying the numbers calculated by using Equations 3.3.1 and 3.3.2, the Carnot efficiency is 85 %, which is the best efficiency that can be obtained under theoretically ideal conditions. As the temperature gets colder the expansion work decreases and the ideal efficiencies increase. The difference between the COP for the pulse tube and the Stirling is that the Stirling can recover some of the expansion work since the expansion piston is mechanically connected to the compression piston.

3.3 Phase shift between pressure and mass flow

3.3.1 Practical Solutions

An important part of the pulse tube function is the heat pumping effect that occurs between the cold-head and the warm end in the pulse tube itself. This effect is greatly enhanced by the phase shifter, which acts to allow heat to be pumped from the cold-head to the warm end heat exchanger to be rejected. The phase shifter provides a phase lag between the oscillating mass of gas moving in the pulse tube (virtual expansion piston) and the compressor piston. The most common hardware is:

- Orifice valve and reservoir
- Inertance tube and reservoir

The aim is to achieve a 90° phase shift between the expansion piston and the compression piston with minimal power loss. The inertance tube provides a more efficient means to achieve the phase shift. The reservoir volume is sized to allow constant pressure in the reservoir so that it acts as on open end, but still maintains the mean gas pressure.

3.3.2 The Helmholtz Resonator

The phase shift mechanism in the pulse tube can be analysed in many ways. As a basic analysis the Helmholtz theory[12] is based on a sphere with a neck out to atmosphere as is pictured in Figure 3.4. The principle behind obtaining resonance from this system is the excitement a mass of gas in the neck (assumed to move as a solid plug) by, for example blowing across it or tapping something down on it. The mass compresses the spring (gas in the sphere) and ends up going further than required for the spring to return it to its original position. Damping exists which serves to degrade the performance of the resonator. This system can be tuned to operate at resonance by using the mass of gas in the neck and the gas spring in the sphere to calculate the frequency required to excite the system.

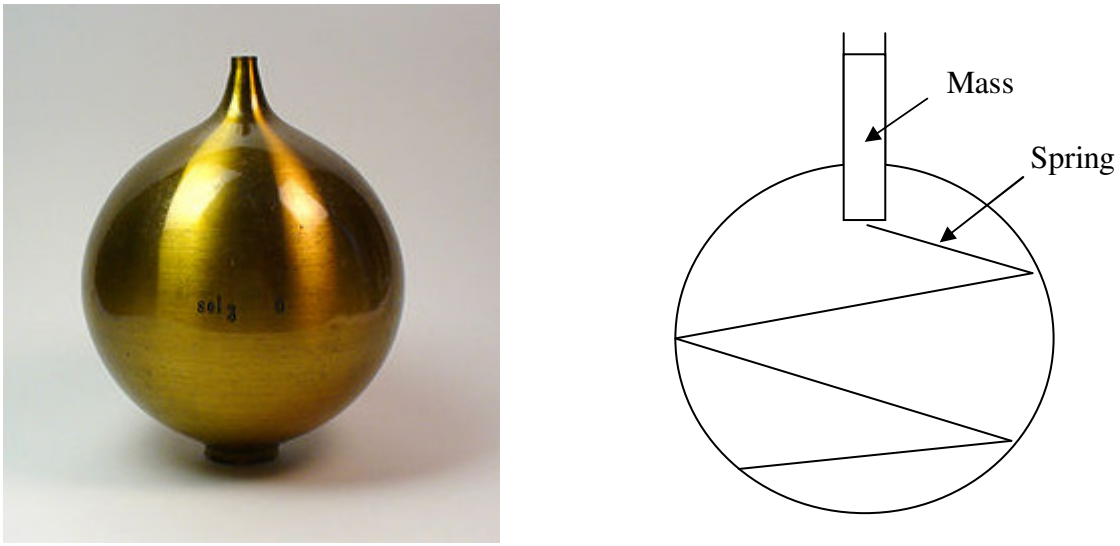

Figure 3.4. Helmholtz resonator

The pulse tube can be considered as a candidate for the Helmholtz theorem of resonance. The inertance tube can be assumed to be a solid plug of gas (mass), and the pulse tube a spring, with the reservoir acting as effectively an open end for the inertance tube. A Helmholtz calculation has been performed with the PT2050 pulse tube. The result was that the resonant frequency was close to 50 Hz with a 4m inertance tube.

3.3.3 Sound Wavelength

Another theory can be applied where a standing wave is generated once a resonance frequency is attained. When a forcing frequency is applied to a system, such as a pressure wave, a longitudinal wave will reflect from perpendicular surfaces. When the resonance frequency is achieved the reflected waves line up with the initial waves and a standing wave is created. Figure 3.5 shows an example of two pipes and standing wave forms. In the open/closed pipe a ¼ wavelength is pictured, where in the open/open pipe a ½ wavelength is shown. The displacement of mass is shown and will be 90° out of phase to the sound waves; therefore the maximum mass flow occur at the open end of the pipe, where the maximum pressure will occur at the closed end or in the centre of the open/open pipe.

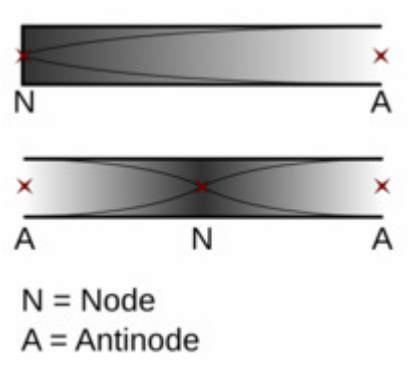

Figure 3.5. Standing displacement waves in open/closed and open/open pipes

A calculation can be performed to determine the ideal length of inertance tube based on standing wave theory. The speed of sound in helium:

$$V = \sqrt{\frac{\gamma \times R \times T}{M}} \qquad \text{Eq (3.4.1)}$$

By placing the properties of helium gas at 300 K into Equation 3.4.1, the speed of sound equates to 1020 m/s. The speed of sound in helium is temperature dependant. However temperature has only a minor impact on the speed over the temperature range found currently in the inertance tube since the velocity is proportional to the square root of the temperature as in Equation 3.4.1. At 250 K the velocity is 930 m/s, and at 350 K it is 1100 m/s. Once the speed of sound is calculated the wavelength can be obtained by dividing by the frequency. For the PT2050, with a frequency of 50 Hz this gives a wavelength of 20 m. To gain maximum amplitude at one end of the inertance tube and minimum at the other a ¼ wavelength of 5 m is required or a multiple of a ¼ wavelength. There are two consequences of increasing the mean pressure: the spring-rate of the gas increases; and opposing this, the density of the gas increases. So in an ideal gas the c_P/c_V ratio, and therefore the velocity of sound, remains pressure-independent.

3.3.4 Electrical Analogy

A method of conducting a more comprehensive analysis of the system is to use an electrical system analogy to the mass, spring and damper mechanical system. This provides a toolbox of well-developed electrical calculations, and programs such as SPICE, to be performed on the system for analysis and optimisation. A very much simplified description of the analogy is provided:

$$F(t) = Damping + \frac{Mass}{Springrate}$$ is the mechanical equivalent of:

$$Impedence = Resistance + \frac{Inductance}{Capacitance}$$

If the system was evaluated for DC flow only: resistance = impedance.

Some features of a cooler, such as the presence of temperature gradients, are effects that the electrical analogy cannot deal with. However, it has been shown to be useful in determining the primary way in which the inertance tube yields the benefits it does[13].

4 Thermodynamic Design of the Pulse Tube Cryocooler

4.1 Sage Model

A numerical 1D model of the pulse tube was created using the pulse tube version of the Stirling (regenerative cycle) simulation software Sage[14]. Sage was used to simulate the performance characteristics of the pulse tube cooler. The description provided by David Gedeon, the author of this software package, is that: "Sage is a graphical interface that supports simulation and optimization of an underlying class of engineering models". Model classes include mass spring damper resonant systems, Stirling-cycle machines, and others. The model is created in a tree like structure: the root of the Sage model of the PT2050 pulse tube is shown in Figure 4.1. In the Sage model the components (icons) are organised in a hierarchical tree structure, where each icon typically contains several layers of other sub-components. For example a component such as a regenerator could contain a metal matrix and an outer tube, and each component can be individually specified in terms of geometry, and numerical data can be entered. The Sage software enables the user to solve, map or optimize the model, and creates output files that can be exported to packages such as Microsoft Excel for further analysis.

The methodology used for designing the pulse tube was to research pulse tubes of similar specification (20 W @ 50 K), and then calculate back from the input power requirement to specify the associated PWG. A Carnot efficiency of 5% was assumed[15], which gave an electrical input power to the PWG of 2 kW for the 20 W @ 50 K of cooling. The final design specification for the PT2050 pulse tube is listed in Table 4.1.

Table 4.1. PT2050 pulse tube design specification

Parameter	**Specification**
Cooling Power	20 W
Temperature	50 K
Carnot COP	5 %
P-V Input Power	1500 W
Working gas	Technical grade helium
Maximum charge pressure	2.5 MPa
Maximum pressure wave amplitude	0.5 MPa
Electrical Input Frequency	50 Hz

The pulse tube was modelled in Sage coupled to a PWG with 60 ml of swept volume. The model for the 7 W at 77 K pulse tube[2] made by IRL was used as a starting point. The initial geometric parameters were based on general relationships[3,16] such as: the cross-sectional area of the pulse tube is proportional to the cooling power requirement; the pulse tube volume is approximately 40 % of the compressor swept volume and the reservoir is approximately 50 times the pulse tube volume. It was found that after optimization, the final model was near the initial conditions mentioned above.

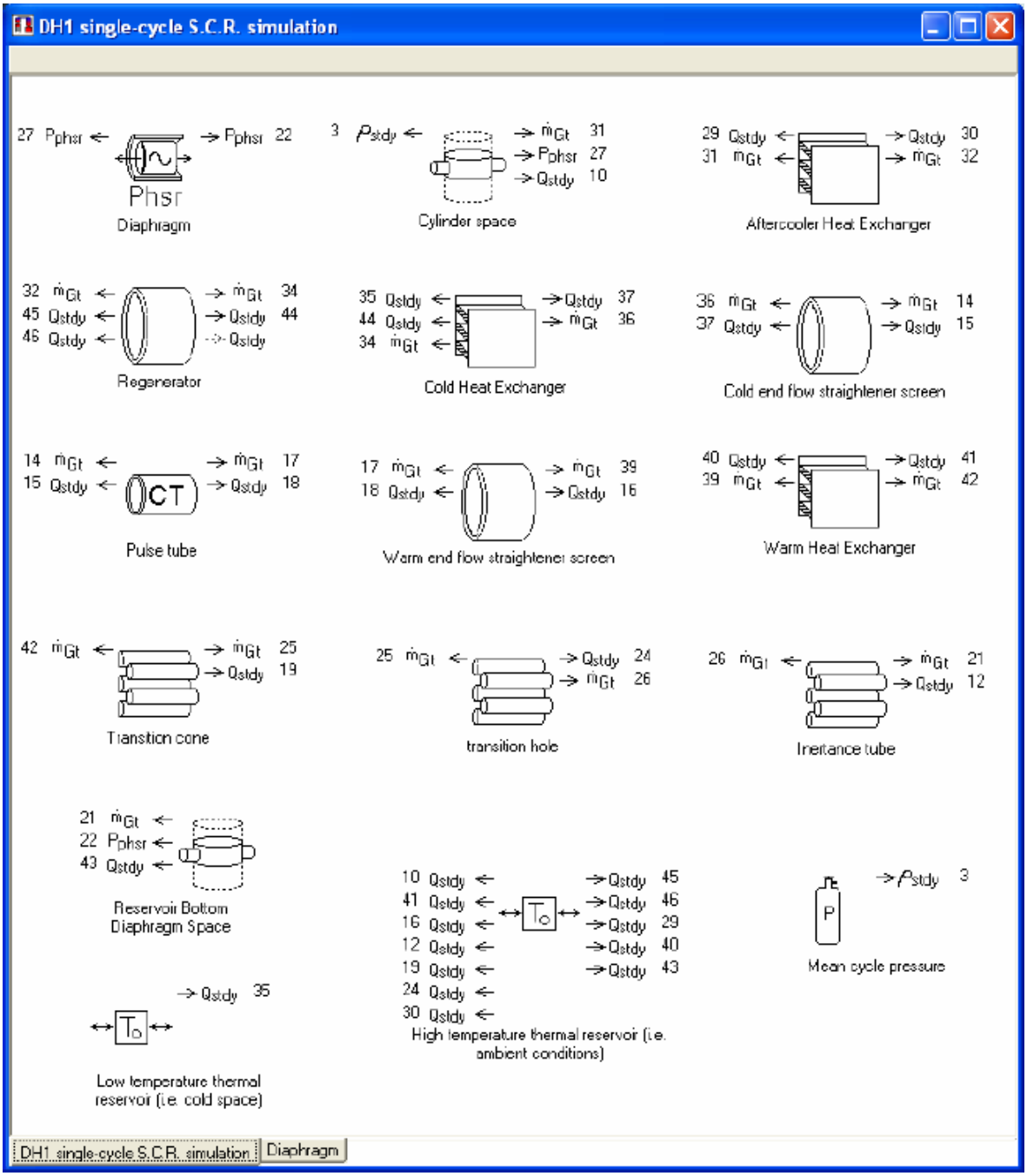

Figure 4.1. Sage model of the PT2050 pulse tube and CHC60 PWG

4.2 Heat Exchangers

Internally slotted water-cooled heat exchangers were used to transfer heat at the aftercooler, coldhead and warm end of the pulse tube. There were three heat flows to consider when designing the heat exchangers: heat transfer from the working gas to the metal; conduction down the fins to the cooling water channels, and heat transfer to the water. The greatest resistance to heat flow was found to be between the working gas and the internal fins.

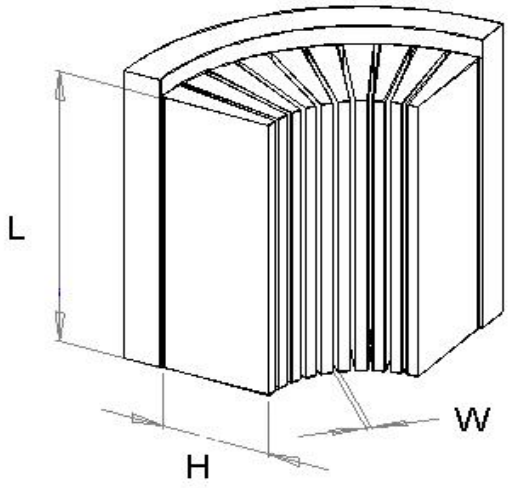

Figure 4.2. Heat exchanger fin slot geometry

The heat exchanger geometry and associated nomenclature are shown in Figure 4.2. Sage model mappings showed that for a given cross-sectional flow area (H x W x n with n being the number of slots), the thinnest slots (W) gave the best cooling performance, if H and n were optimized. It was found that several compromises were necessary. Thinner slots increased the pressure drop across the heat exchanger (negative), heat transfer increased (positive), dead volume decreased (positive), and the cost of the fin wire-cutting operation increased (negative). The minimum slot width was eventually determined by practical wire-cutting limitations. The heat exchanger length (L) also contributed to the flow result, with longer lengths (L) requiring an increased flow area since a higher pressure drop will occur with longer length where increasing the flow area reduces the pressure drop.

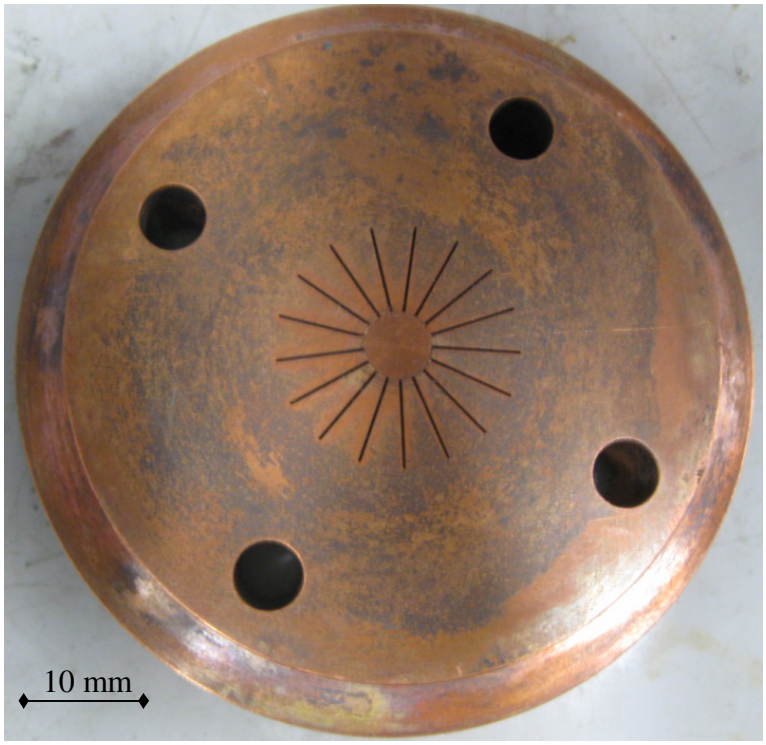

Figure 4.3. Warm heat exchanger.

Sage was used to optimise the gas transfer geometry and Cosmos finite element analysis (FEA), described later in this chapter, was used to look at heat conduction down the fins. A variety of fin configurations were analyzed for efficient conduction such as a tree type arrangement, tapered fins and different fin angles. The taper on the fins allowed a more uniform heat flux down the fins to the base as they gained (or gave) energy from the flow. The highest heat conduction was found for the thinnest slot (W) due to the larger quantity of metal that remained for conduction. It was found that radial slots gave the best result. A relatively large centre hole was required to accommodate the number of slots and slot width yet allow enough fin material to hold a plug. Figure 4.3 shows the copper warm end heat exchanger that was used in the pulse tube.

4.3 Assumptions in the Sage Model

The Sage model created for the PT2050 was primarily a 1D model, with some 2D thermal flows. Therefore some assumptions were made within the Sage model, which include: 3D fluid and thermal flow losses throughout the pulse tube were assumed

negligible; Radial heat transfer in the regenerator mesh is negligible; Thermal streaming (re-circulating flow loss) in the regenerator is negligible; Acoustic streaming (another re-circulating flow loss) in the pulse tube is negligible. The water-cooling to the warm heat exchanger and after-cooler was assumed to provide an isothermal surface. Some of these assumptions may not be correct, and together are likely to predict a better performance than observed. Moreover, the output cooling power in the Sage simulation did not include heat leaks along sensor wires, heat leaks from conduction through gas (non ideal vacuum), heat leaks from conduction along the Multi Layer Insulation (MLI) and radiation heat leaks. Some of the thermal leaks have been experimentally measured and also estimated, and are discussed in Section 7.2.

4.4 Refinements to the Sage Model

Several improvements were made to the initial Sage model: the internal heat exchangers were changed from channel type to fin type; various outputs were cross-referenced, such as heat exchanger cross-sectional areas in the output files to calculated areas to account for the tapered fins; and changing surface types to suit thermal wavelength versus wall thickness. These modelling changes were made based on the Sage 6 manual[14].

A sensitivity analysis was conducted and it was found that the model was sensitive to the mesh size parameter (Ncells) in the pulse tube component. Ncells was mapped to determine a value close to the asymptotic value, whilst remaining computationally efficient.

Convergence times with the model were reasonable at around 30 seconds per run. Computation time with approximately 5 parameters to map was up to 15 minutes. It was found that the sensitivity of various parameters in the model could change if, for example, another parameter is added, or even changed. An attempt has been made to find the inter-dependency of each parameter within the model, and some of the more important findings from this are now discussed.

Figure 4.4 compares the cooling and input performance between the initial Sage model, which was used to predict the performance of the PT2050 at the design freeze, versus the refined model (post design and manufacture). The initial model predicted 30 W of cooling power at 50 K; with 1800 W of p-V input power. The final Sage model predicts 38 W of cooling power at 50 K for a p-V power input of 1500 W.

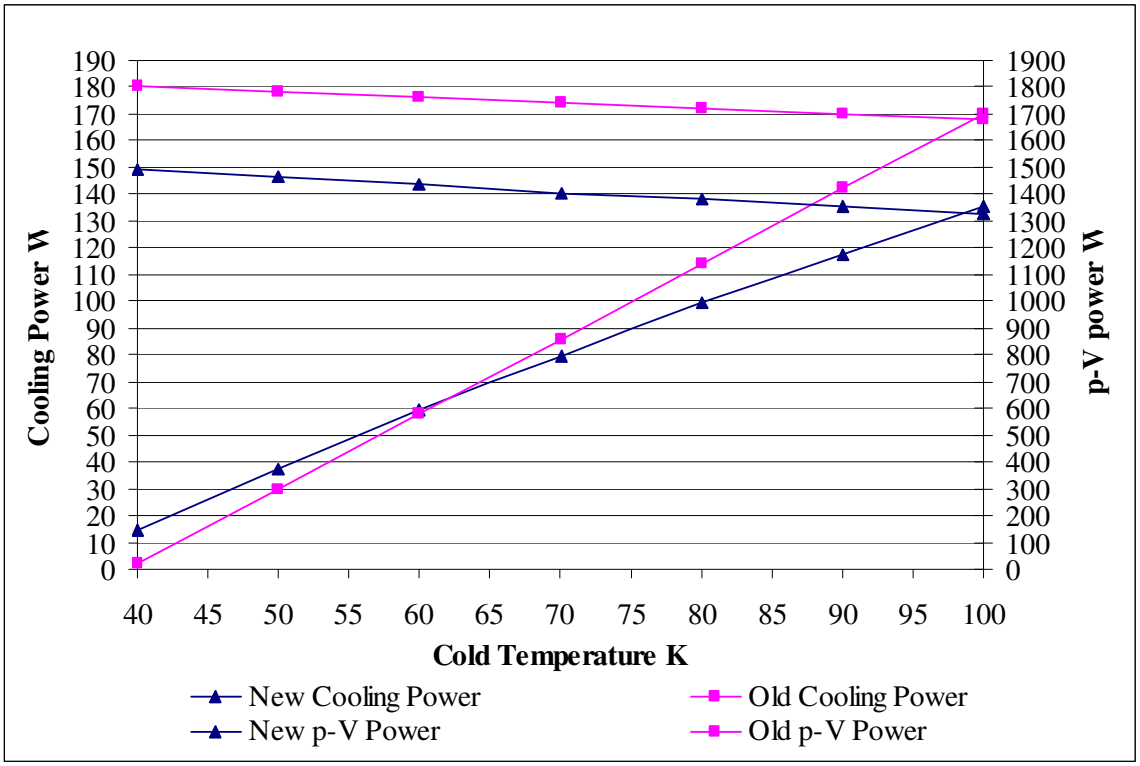

Figure 4.4. Comparison between the initial and refined Sage models

4.5 Thermal Analysis

4.5.1 Calculations

Some calculations were carried out to validate the Sage model. These are included in Appendix B. An experimental measurement and some estimates of the thermal leakages in the system are included in Chapter 7.

4.5.2 Finite Element

A Cosmos thermal analysis was carried out to determine an optimum shape for the internal fins of the three heat exchangers, in terms of heat transfer. A 2D convective model was created for comparison purposes, assuming a convective coefficient of 100 W/m^2 K. The shape that gave the smallest radial temperature difference, from the shapes trialled, was the radial slotted heat exchanger as shown in Figure 4.5. An isothermal surface at 295 K at the outer water-cooling slots was assumed. A solid plug was fitted into the central hole. The highest temperature is shown at the tips of the fins, which is expected since the heat flow is restricted at the root of the fins due to the amount of heat needing to pass through at that point (the sides of the fins allow heat to transfer into the fin along their lengths).

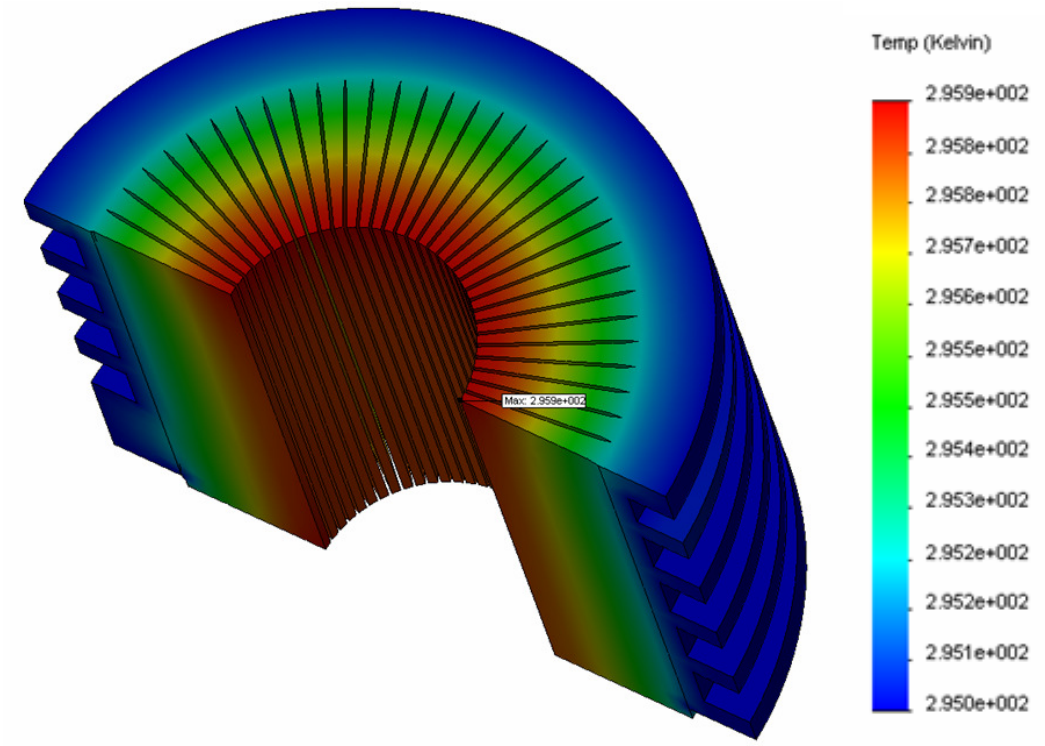

Figure 4.5. Cosmos temperature gradient in after-cooler heat exchanger

5 Design and Fabrication of Hardware

5.1 Cryocooler

The cryocooler (Figure 5.1) was manufactured in Christchurch, New Zealand using standard machine shop equipment. For the purposes of the overall project the refrigerator has been split into a PWG (a design and build task undertaken by others in an associated project) and the pulse tube (which is the focus of the project described here). A CAD model of the pulse tube, developed in Solidworks®, was based on the component geometries obtained from the optimised Sage model simulations (Chapter 4). The pulse tube has been designed to couple directly on top of the PWG's top plate, with the entrance of the copper after-cooler as close as possible to the diaphragm.

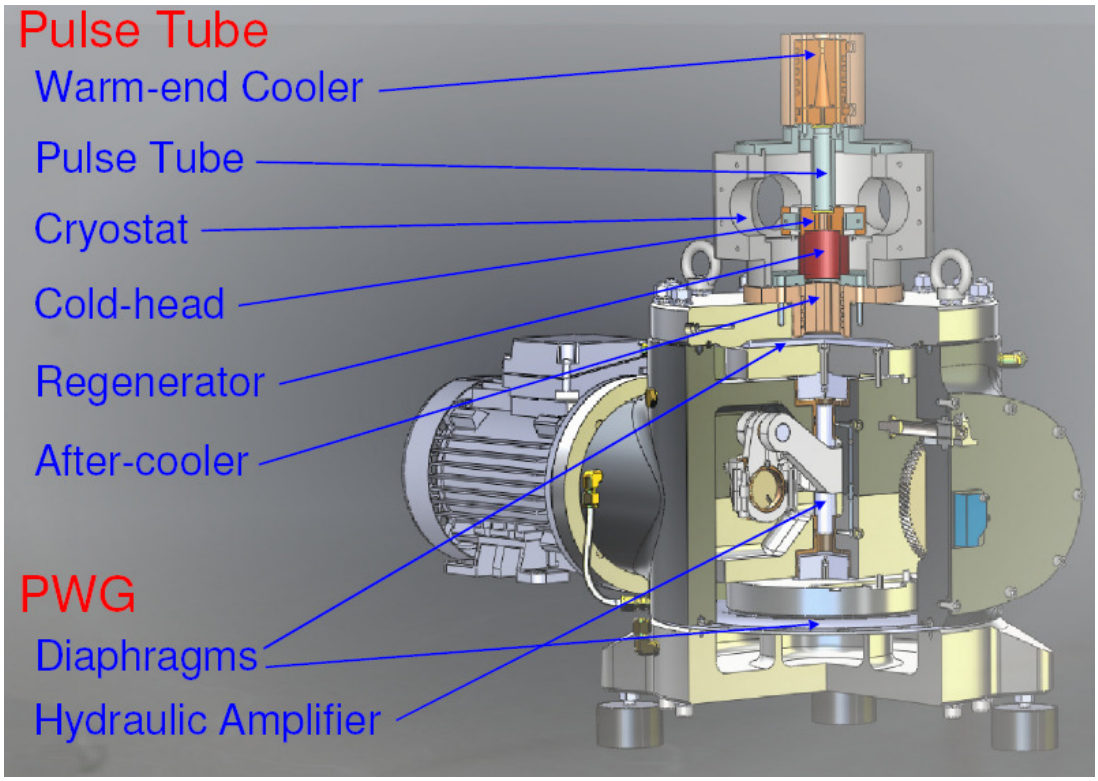

Figure 5.1. Cryocooler - CHC60 PWG and PT2050 pulse tube.

5.2 Pressure Wave Generator

Power is delivered to the pulse tube by way of a diaphragm PWG (Figure 5.1), which successfully separates the driving mechanism's lubricating oil from the pulse tube working gas. The diaphragms are placed opposite each other to cancel out the force on the mechanism due to the mean gas pressure, thereby leaving only the fluctuating force due compression for the bearings to react. Since the diaphragms have a relatively large area the stroke requirement to achieve the specified volumetric displacement is quite small (approximately 1.6 mm).

The CHC60 PWG incorporates a hydraulic drive mechanism and a cast crankcase, which have been developed at IRL. The hydraulically actuated master/slave piston assembly was used to reduce the crankshaft stroke of 16 mm to 1.6 mm and amplify the force. This PWG was developed in parallel to the PT2050 at IRL. The final specification for the PWG is shown in Table 5.1.

Table 5.1. PWG design specification

Parameter	**Specification**
Displacement	60 cc approximately sinusoidal
Dead volume	80 cc
Max motor shaft power	2.2 kW
Frequency	Up to 60 Hz
Maximum charge pressure	2.5 MPa
Maximum pressure wave amplitude	0.5 MPa

The PWG has a speed controller connected to a 2 pole 3-phase motor. The speed controller allows the system frequency to be varied for tuning purposes, and can be run up to about 60 Hz, limited by internal dynamic PWG bearing loads.

5.3 Pulse Tube

The pulse tube design started with the geometry obtained from modelling work detailed in Chapter 4. A design loop was created between manufacturing possibilities and best performance in theory. This resulted in detailed drawings being sent to a commercial workshop to manufacture the components.

5.3.1 Material Strength

The pulse tube was designed to withstand a design pressure of 3 MPa. Although the energy contained in the system due to the pressure and volume was low, a conservative approach was taken. The thin walled tubes, diameters 21 and 44 mm with 0.4 mm wall thickness, were designed with a factor of safety of 5 (typical of pressure vessel standards). This factor of safety could be lowered to minimise thermal leakages by reducing the wall thickness in the pulse tube and regenerator tube.

5.3.2 Component Design

Figure 5.2 shows a SolidWorks® CAD model cross-sectional view of the PT2050 pulse tube. The inertance tube connects at the top of the pulse tube and ends at an enclosed reservoir. The pulse tube assembly bolts on top of the PWG.

The design intent was to create a tuneable pulse tube with as much modularity as possible. The cold-head interface with the pulse tube and regenerator was soldered, since a cold seal at this point was deemed a difficult task based on previous experience at IRL. The after-cooler heat exchanger was also soldered to avoid the risk of helium leakage into the coolant. The other component interfaces were bolted and sealed with o-rings so that the pulse tube could be disassembled without difficulty.

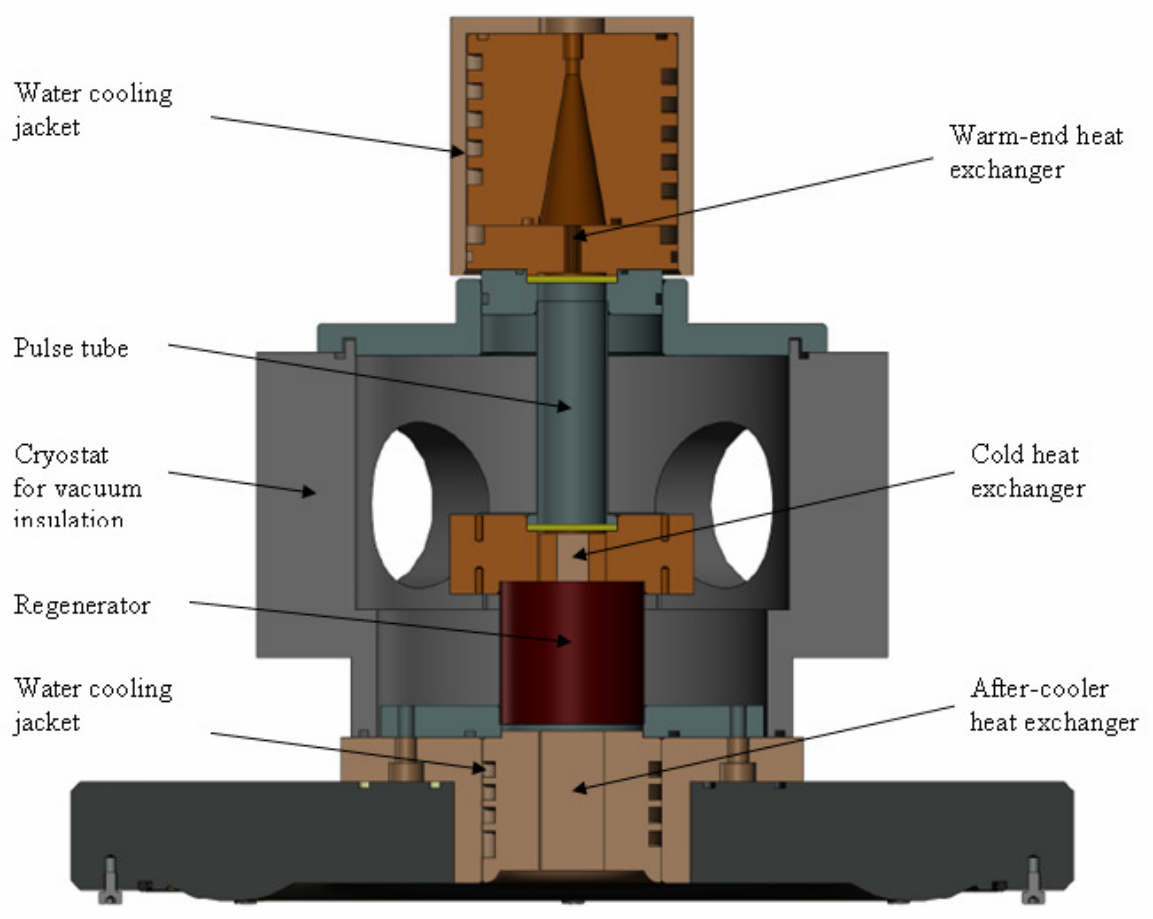

Figure 5.2. Cross-sectional view of the PT2050 Pulse tube.

Heat Exchangers

The heat exchangers were machined from copper with wire-cut internal fins (Figures 4.3, 5.4 and 5.6). A central plug was shrunk with liquid nitrogen before it was fitted into the centre of the heat exchangers. The fins slots were specified at 0.25 mm and were measured after manufacture to be 0.17, 0.19 and 0.22 mm wide for each of the three respective heat exchangers.

Helical grooves were cut in the outer material of the warm-end and after-cooler heat exchangers to enable cooling fluid to be pumped through to remove heat. Figure 5.3 shows the helical groove cut in the warm-end cooler. The after-cooler heat exchanger had two helical cuts starting 180° apart. The two helical grooves were joined at the

bottom to allow cooling fluid to be fed in through the upper flange of the after-cooler assembly.

Figure 5.3. Aluminium transition cone with cooling grooves

The cold heat exchanger had holes drilled and tapped for fitment of temperature sensors and resistance heaters. The holes were cross-drilled to allow evacuation of gases trapped beneath the bolts. The heaters were clamped to the four sides of the cold-head, and were used to provide a cooling load for the pulse tube during testing, as described in Section 6.2.5.

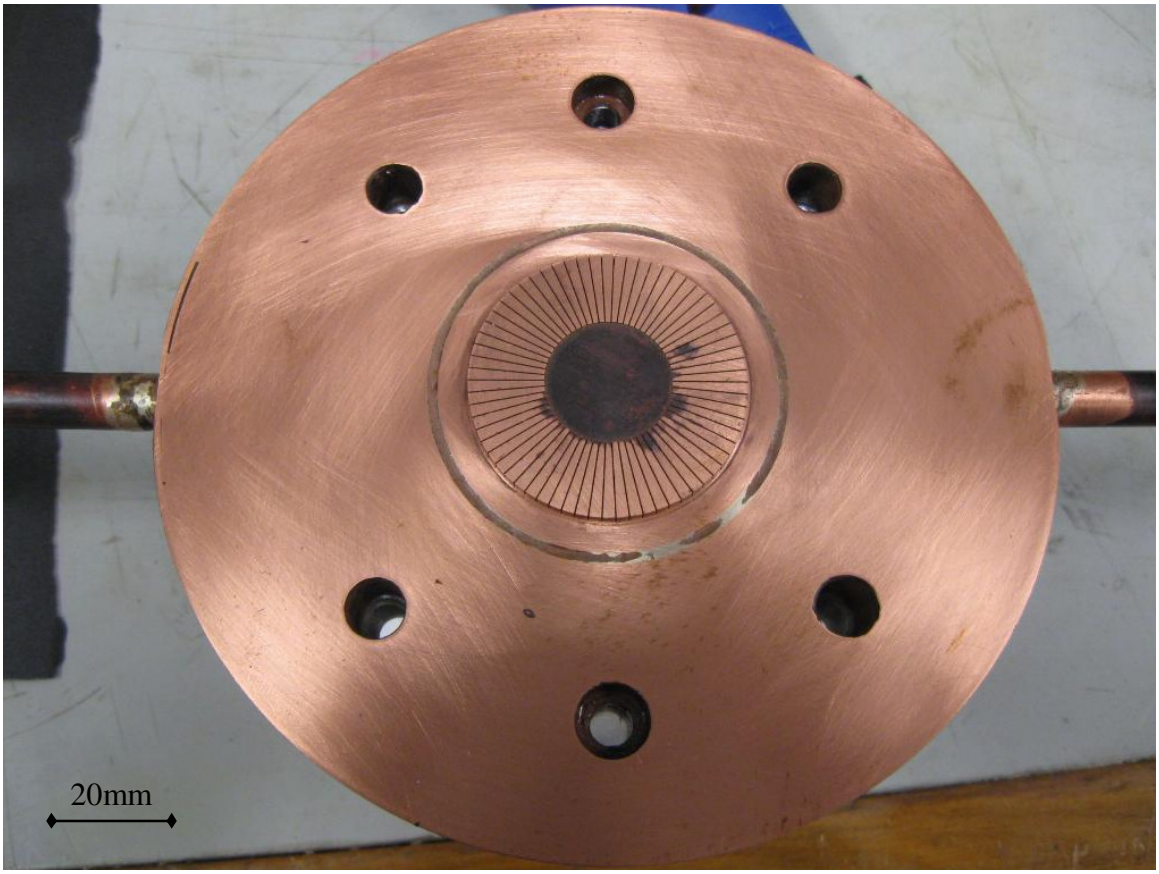

Figure 5.4. After-cooler heat exchanger assembly

Pulse tube

The pulse tube was fabricated from a standard stainless steel tube with internal diameter of the correct size, so only the outside diameter required machining. The pulse tube was 76 mm long with a wall thickness of 0.4 mm and inside diameter of 21 mm.

Inertance tube

A copper inertance tube with an inside diameter of 4.3 mm and a 1 mm wall thickness was used with lengths of 2 m (Sage predicted optimum length) and 4 m (found subsequently to give better performance experimentally).

Figure 5.5. Stainless 400-mesh (left) and brass 100-mesh (right) laser cut discs (after being removed from the pulse tube subsequent to a solder repair - the reason for the concentric heat markings around the centre that can be seen in the photo)

Regenerator

The core matrix of the regenerator was created from 794 individual stainless steel 400-mesh discs laser-cut from sheet. Figure 5.5 shows the regenerator discs on the left; the discs on the right are flow straighteners, which are described in the next paragraph. The material is generally used as a filter, which is the common application in industry. The mesh stack was housed in stainless steel tubing, as shown in Figure 5.6. The tube was 47 mm long with a 44 mm inside diameter, and had a 0.4 mm wall thickness to reduce thermal losses down the length of the tube. The number of discs required was calculated from the diameter of two of the wires in the mesh (0.03 mm) and the length of space available for the mesh. The as-supplied regenerator mesh was shadow-graphed and the diameter was found to be undersize by about 0.5mm. It was decided, however, to

proceed with the undersize mesh. In future development, if the process of sizing the tube is easier than accurately cutting the mesh, it may be more effective to machine the tube subsequent to the mesh being laser-cut.

Flow straighteners

Brass 100-mesh discs, pictured on the right of Figure 5.5, were laser cut from sheet to serve as flow straighteners to settle the gas flow entering and leaving the pulse tube. A small plenum was manufactured between the heat exchangers and the mesh to aid in the straightening effect. A compromise existed between straightening the gas flow and reducing the pressure drop created by the mesh.

Figure 5.6. Cold heat exchanger looking down the regenerator tube

The regenerator and flow straightener mesh wire diameter and number of mesh were measured, from which the porosity value was calculated for entering into the Sage model for further refinement.

Reservoir

An existing 2.3 litre reservoir (Figure 5.7) was used for experiments. The eventual aim is to make use of the PWG's gas spring as the reservoir, since the pressure wave in the gas spring is small.

Figure 5.7. 2.3 litre reservoir

5.4 Insulation

Since the cold-head can operate at temperatures around 50 K, and ambient is around 300 K, there is a very significant temperature difference of 250 K to drive heat to the cold-head. Being aware of, and mitigating against the 3 modes of heat transfer was a requirement.

Conduction/convection in gas

A cryostat enabled a volume around the pulse tube to be sealed from atmosphere so that a vacuum could be applied around the cold head of the pulse tube to minimise the heat leak from ambient caused by conduction and convection via air molecules. A pre-existing cryostat was adapted to fit the PT2050 pulse tube arrangement, as shown in Figure 5.8, during the design process. The cryostat was sealed using o-rings. Four NW50 (5 mm diameter hole) ports allowed vacuum fittings to be attached for the connection of vacuum pumps, vacuum gauge, and a power feed-through for the instrumentation (Temperature, heater power, etc).

A vacuum of at least 10^{-5} millibar was considered necessary for the initial testing, to reduce thermal leakages. A mechanical vacuum pump and a diffusion pump served the purpose of ensuring the required vacuum was maintained. The system was left running for several days after an assembly to allow out-gassing of any residual contaminants to take place.

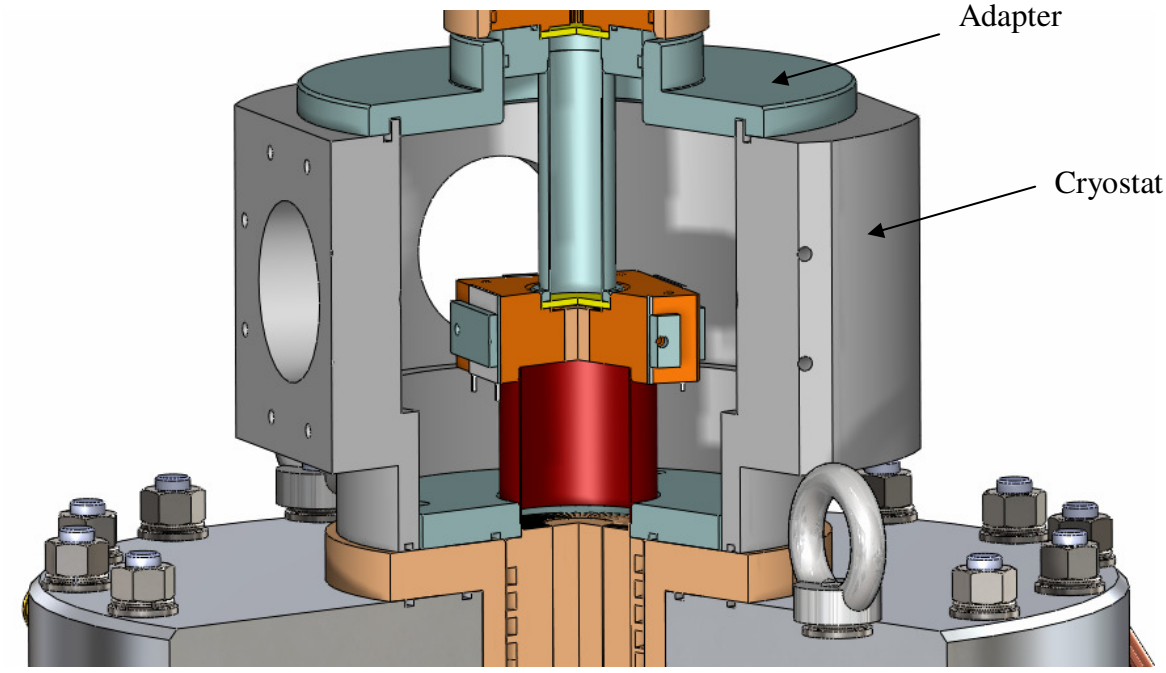

Figure 5.8. PT2050 cryostat arrangement

Conduction in solid components

The primary conduction paths were: the regenerator tube and pulse tube which join the cold-head to the two warm heat exchangers; the regenerator matrix and sensor and heater wires.

The tubes were made from stainless steel to help reduce conduction. A minimal wall thickness (about 0.4 mm) was left to minimise (as much as structural requirements would allow) axial conductive heat transfer from the adjoining flanges to the cold-head.

The regenerator matrix was made from stacked screen mesh discs, as opposed to cylindrically wound ribbon, to reduce axial heat conduction from disc to disc.

The calculation for heat leak from temperature sensor wires and heater current wires is shown in the Appendix. This calculation was performed to optimise the conflicting consequences of reducing the wire diameter: while thinner wires are a smaller conductive path they have a higher electrical resistance with consequently increased Ohmic heating. It was found that the compromise in the sensor wires was dominated by thermal losses, since electrical currents were low, whereas the heater wires had relatively higher electrical currents.

Radiation

The surfaces of the pulse tube assembly that were inside the cryostat, as well as the inside of the cryostat itself, were polished to lower the absorption and emission of radiation heat energy.

Multi Layer Insulation (MLI) blanket was used to provide radiation shielding. The MLI blanket is typically made up of several aluminized Mylar sheets with a layer of Dacron, a polyester based product, between each sheet. Dacron minimises conduction between each layer of the MLI blanket and can also be used to insulate between surfaces and the MLI.

6 Cryocooler Assembly, Instrumentation and Laboratory

6.1 Assembly

6.1.1 Cleaning

The pulse tube was polished and washed in acetone in an ultrasonic cleaner under a fume hood; the set-up is shown in Figure 6.1. The mesh discs were cleaned using the same procedure. The components, including the mesh discs, were then oven-dried at 50°C overnight, and then assembled with o-rings and internally evacuated under vacuum overnight to help to remove any remaining residue.

Figure 6.1. Ultrasonic cleaner set-up for cleaning the pulse tube components

6.1.2 Soldering

The pulse tube was soldered together at the joints between the pulse and regenerator tubes and at the water to gas joints in the after-cooler heat exchanger. The soldering process involved using a high silver content solder (45%) with an appropriate flux (Hi-Tenacity 6). The components were placed in a jig to hold them straight, with axial pressure applied to hold the warm end flow straightener brass discs in place. Furnace brazing was attempted, but unfortunately the process was not entirely successful due to the flux corroding the outer surfaces of the thin-walled (0.5mm) pulse tube and also the equally thin-walled regenerator tube. Figure 6.2 shows the damaged surfaces.

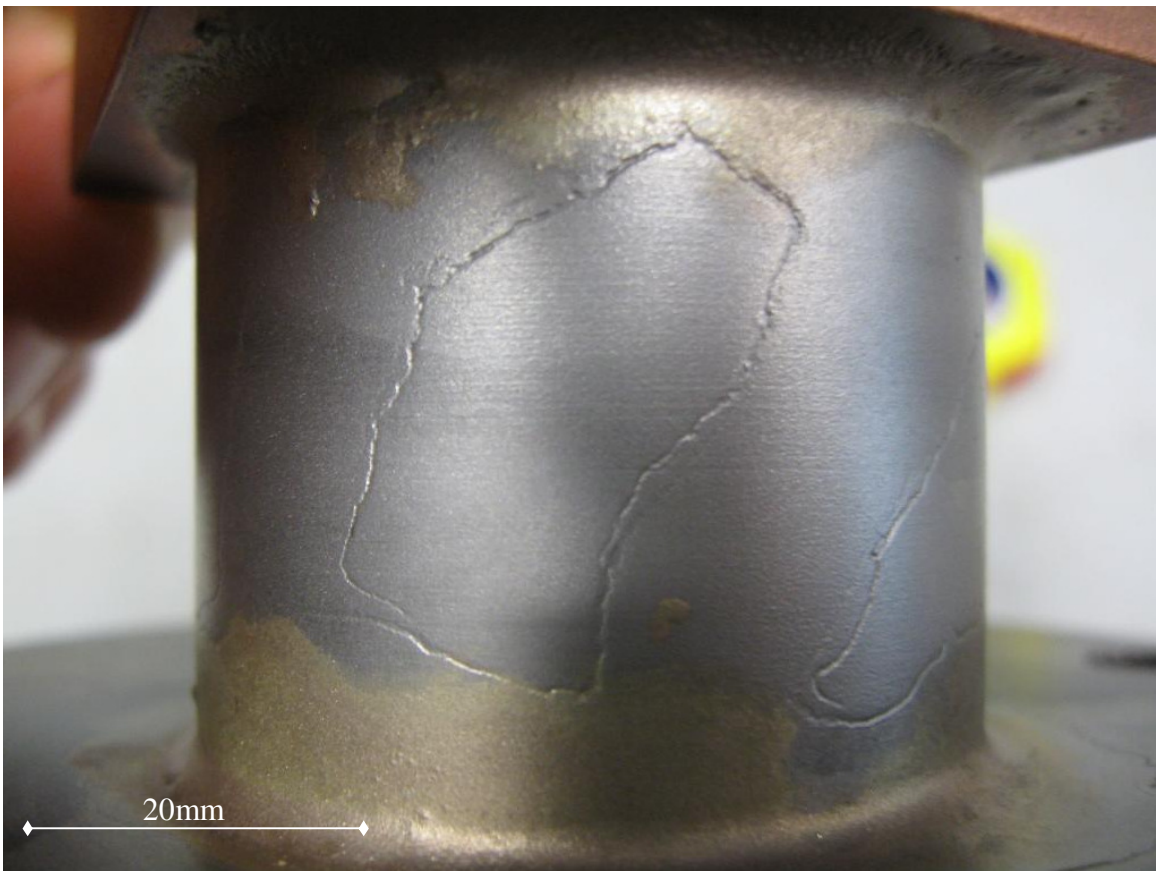

Figure 6.2. Damage due to soldering flux on thin walled regenerator tube

The outer surfaces of the pulse tube were then polished to reduce radiation heat losses. This process created another problem: one of the soldered joints leaked helium into the cryostat. Re-soldering the joint in the area that was leaking sealed the hole. Due to time

constraints it was decided to leave the regenerator mesh in place during the soldering process. An argon bottle with a regulator from a TIG welding set was connected to the pulse tube to run argon gas through the pulse tube assembly, which is common practice to minimise oxidation and scaling on the inside of externally welded components. Unfortunately the gas was not applied as soon as the soldering took place, but approximately 20 seconds after.

Once the joint was soldered a quick pressure check revealed a leak further around on the same soldered connection. It was decided to re-solder around the entire circumference of the joint. The argon gas was discovered to be escaping through the molten solder and thereby creating a porous joint, which explained why the joint leaked in an area adjacent to the first repair. The solution was to turn the argon gas flow on for a few seconds, then off when soldering to reduce the gas pressure inside of the assembly.

The pulse tube was used to conduct experiments, and then stripped for inspection. The discs near the solder repair were discoloured and there was evidence of contaminants coming from the heat exchanger. Figure 6.3 shows the discolouring and contaminants caught up in the regenerator mesh. Depending on the amount of damage, individual discs were either replaced, or cleaned and reused.

6.1.3 Regenerator and Flow Straighteners

The mesh discs were weighed with high accuracy scales in sets of 10, 20 and 30 to obtain an average value for the mass of an individual disc, and also the consistency of measuring them. This proved to be an accurate way of measuring the number of discs in a stack, so that they then did not have to be counted up individually. The discs were then assembled in random orientations. A press was used, along with a close fitting press tool (Figure 6.4), to compress the stack of discs to make the assembly easier. A strength calculation on the regenerator tube was carried out to prevent damage due to stress from pressing,

and the discs were compressed only to their fitted position down the tube, so as to avoid damage to the regenerator tube. Even with the press it was found that the discs protruded the opening after the press force was removed, and required some careful manipulation to assemble the after-cooler that was designed with clamping bolts to compress the discs.

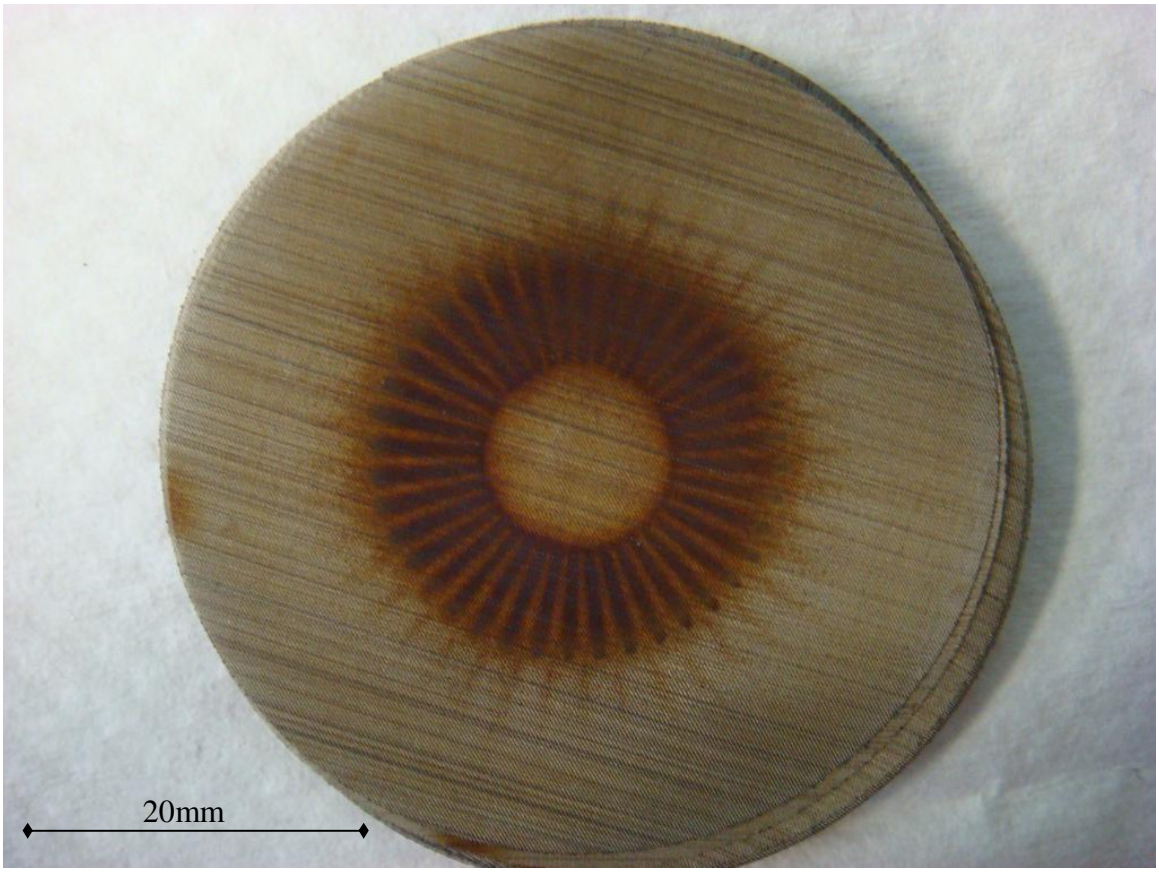

Figure 6.3. Regenerator mesh pattern after use

The flow-straightener mesh discs were counted up based on their mesh wire diameter and stack height required. A pneumatic pressure test to 3.5 MPa was carried out in a controlled environment to check if the vessel could withstand the design pressure plus a margin.

Figure 6.4. Regenerator press tool

6.1.4 O-ring Sealing

The pulse tube was designed to have the split joints with their respective o-rings placed away from the cold-head, to avoid having to seal at cryogenic temperatures. The o-rings used were nitrile (NBR) 70 Shore hardness, and were a cast type o-ring (with the circumferential flash as opposed to the joined extruded type). Viton o-rings were considered as a higher quality o-ring, but for the purposes of the tests done, nitrile seemed to have sealed sufficiently well. High vacuum o-ring grease was used sparingly on the o-rings in the cryostat and pulse tube to minimise out-gassing in the cryostat and pulse tube.

The o-ring surfaces on the components were polished in a circumferential direction to remove scale and create a nice smooth surface for sealing the helium, air and water from each other. This finishing detail was carried out in-house at IRL, and also included creating some radii and minor resizing of some components to allow for correct assembly.

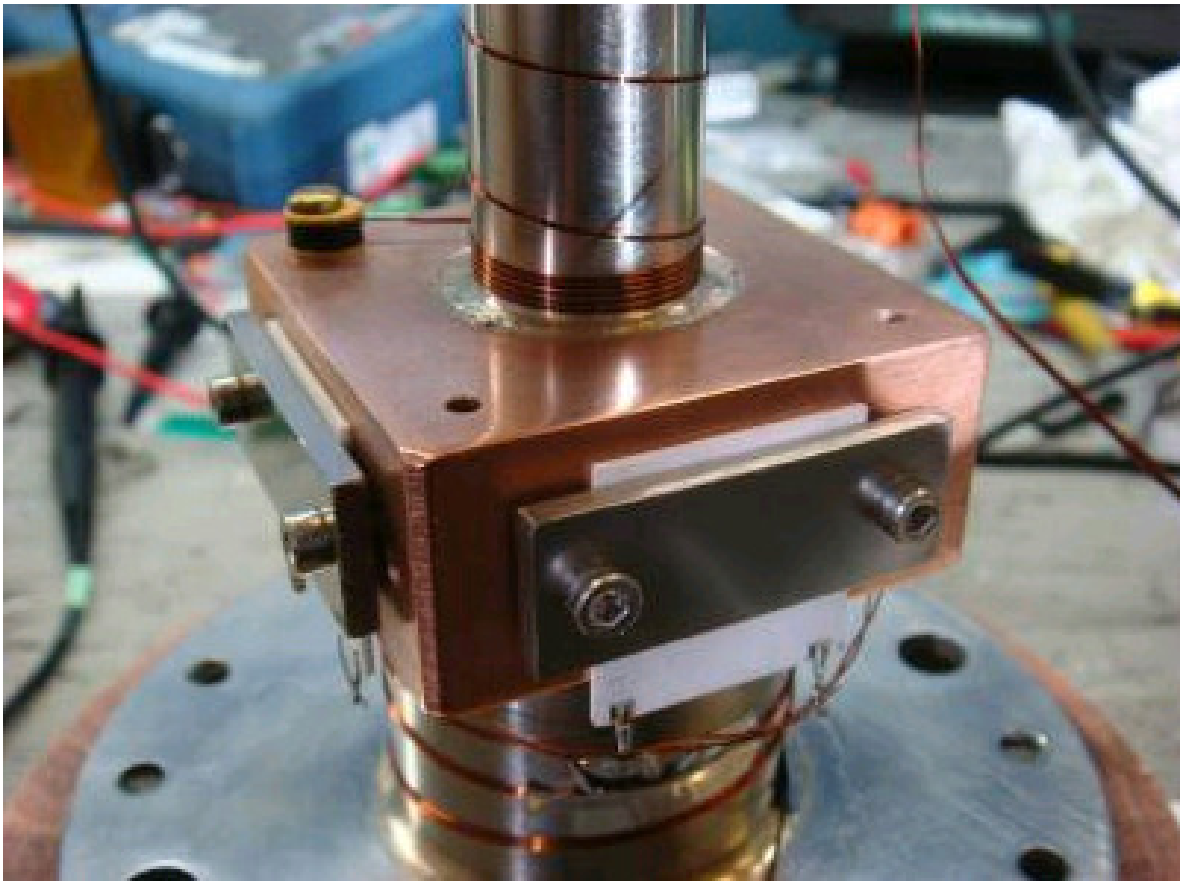

Figure 6.5. PT2050 pulse tube wired with heaters and a temperature sensor

6.1.5 Cold-head Insulation

Figure 6.5 shows the pulse tube assembled, and ready to have Dacron and MLI applied. The MLI blanket needed to be placed loosely to prevent conduction between layers, with no more than 30 layers placed per centimetre, as a rule of thumb. Some heat transfer does occur with MLI through conduction along its length, hence a longer length wrapped around or several individual layers on top of each other is a good option. A vacuum was necessary for the MLI function to minimise conduction/convection through the atmosphere between the layers of MLI.

Dacron sheet was cut to size and then wrapped around any component where the MLI might contact to reduce thermal conduction to the MLI. The 10-layer MLI blanket came

prepared with Dacron between layers to help prevent conduction from one layer to the next. Reflective tape was used to connect every third layer of the blanket and to attach the MLI to the pulse tube assembly. It was also used to anchor the sensor and heater wires to the regenerator and pulse tubes. Figure 6.6 shows the pulse tube assembly, with MLI blanket and Dacron in place, ready to be assembled with a cryostat on the PWG.

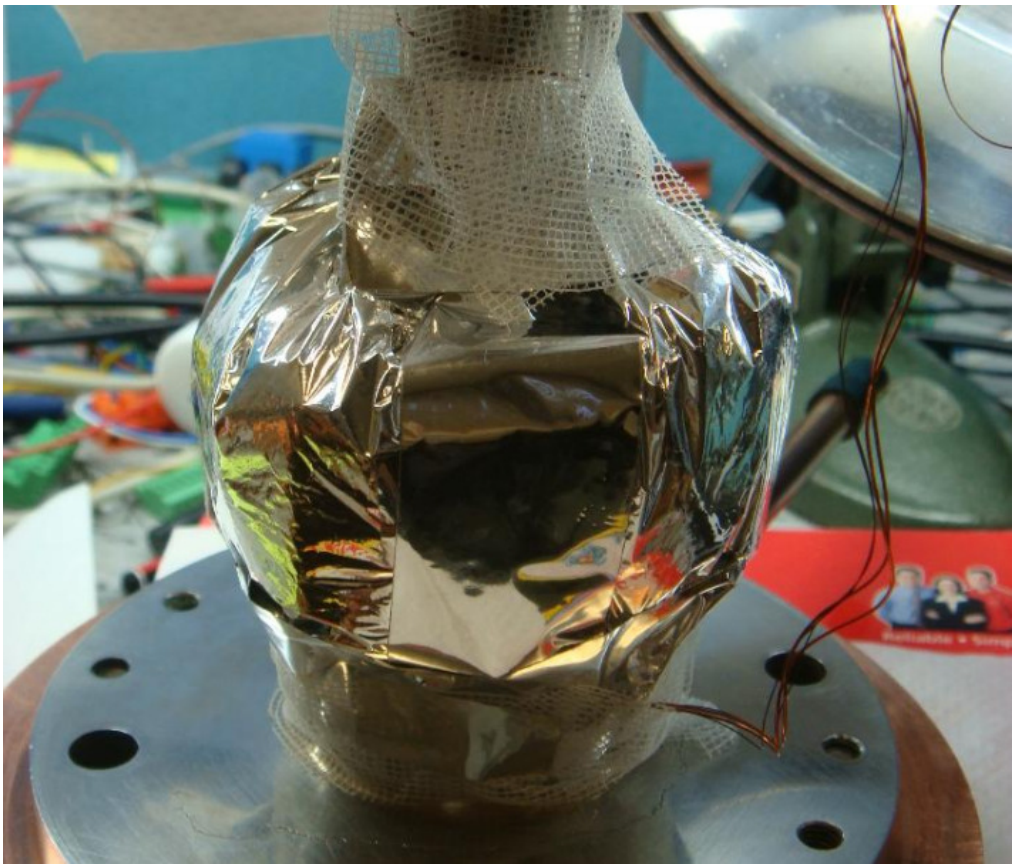

Figure 6.6. Pulse tube assembly with Dacron and MLI insulation

6.2 Instrumentation

6.2.1 Temperature

The cold-head temperature was measured with a calibrated Lakeshore DT-670 silicon diode[17] and a PT100 platinum sensor. Brass screws were used to mount the sensors so that the thermal expansion was matched between the bolts and the sensors. A cryogenic heat-transfer paste was used to help transfer the heat from the cold-head to the sensors.

Both sensors used a four-wire measurement, thermally anchored by winding the leads up the pulse tube. A Lakeshore 218 eight channel temperature monitor was used to measure the cold temperatures. Type T thermocouples were used to measure the after-cooler, block, warm-end and PWG oil temperatures.

6.2.2 Displacement

The PWG slave piston position, and hence the diaphragm stroke, was measured with a laser sensor (Keyence LB-72). A previous experimental correlation at IRL, using a CHC200 PWG, between the fluid volumetric displacement and the effective area of the diaphragm showed that the effective area of the diaphragm is very close to the diameter that is in the centre of the circumferentially swaged recess in the diaphragm (Figure 6.7). The correlation involved measuring fluid displacement from the PWG at different crank angles. The maximum measured fluid displacement gave the same output as a displacement calculation based on the effective area and stroke. The effective diameter of the CHC60 diaphragm was used to calculate the displacement from the measured stroke of the running machine.

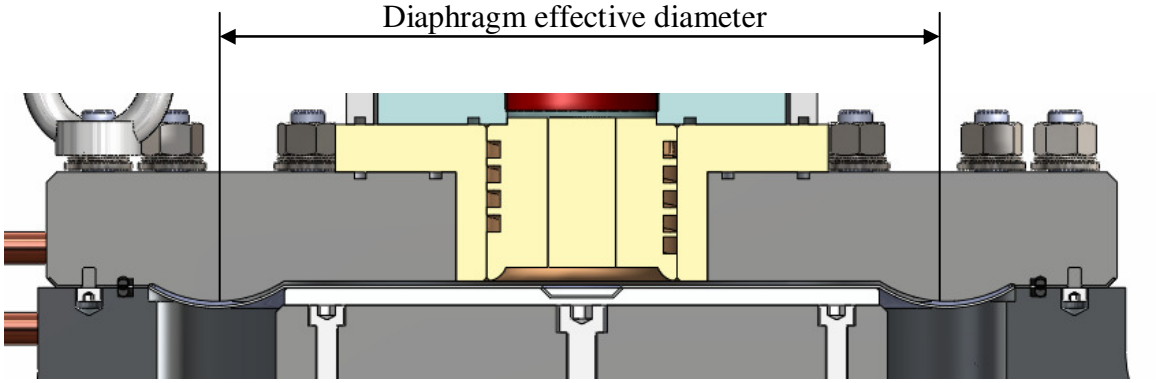

Figure 6.7. Diaphragm configuration

6.2.3 Pressure

A Sensor Technics PS20500G pressure transducer was used to measure the pressure in the compression space of the PWG. The sensor was tapped into the top plate on the pulse tube's side in the recess of the diaphragm and in the axis of the slave piston. PTX 7517-3257 pressure transducers were also used at either end of the inertance tube, i.e. at the

reservoir and at the warm end of the pulse tube. All of the pressure sensors measure gauge pressure (i.e. they include atmospheric pressure in the final output).

6.2.4 Data Acquisition

The sensors provided inputs to a National Instruments SCXI signal conditioner and were processed on a computer. An IRL-developed program, using Lab windows software, was used as a real-time indicator of performance, as well as to capture the data for post-run analysis. A sampling frequency of 16 kHz was used. The graphical interface is shown in Figure 6.8. Microsoft Excel software was used to analyse and present the data. Sensor outputs provided a real-time pressure ratio (ratio of maximum to minimum pressure), displacement and a p-V loop (indicated power).

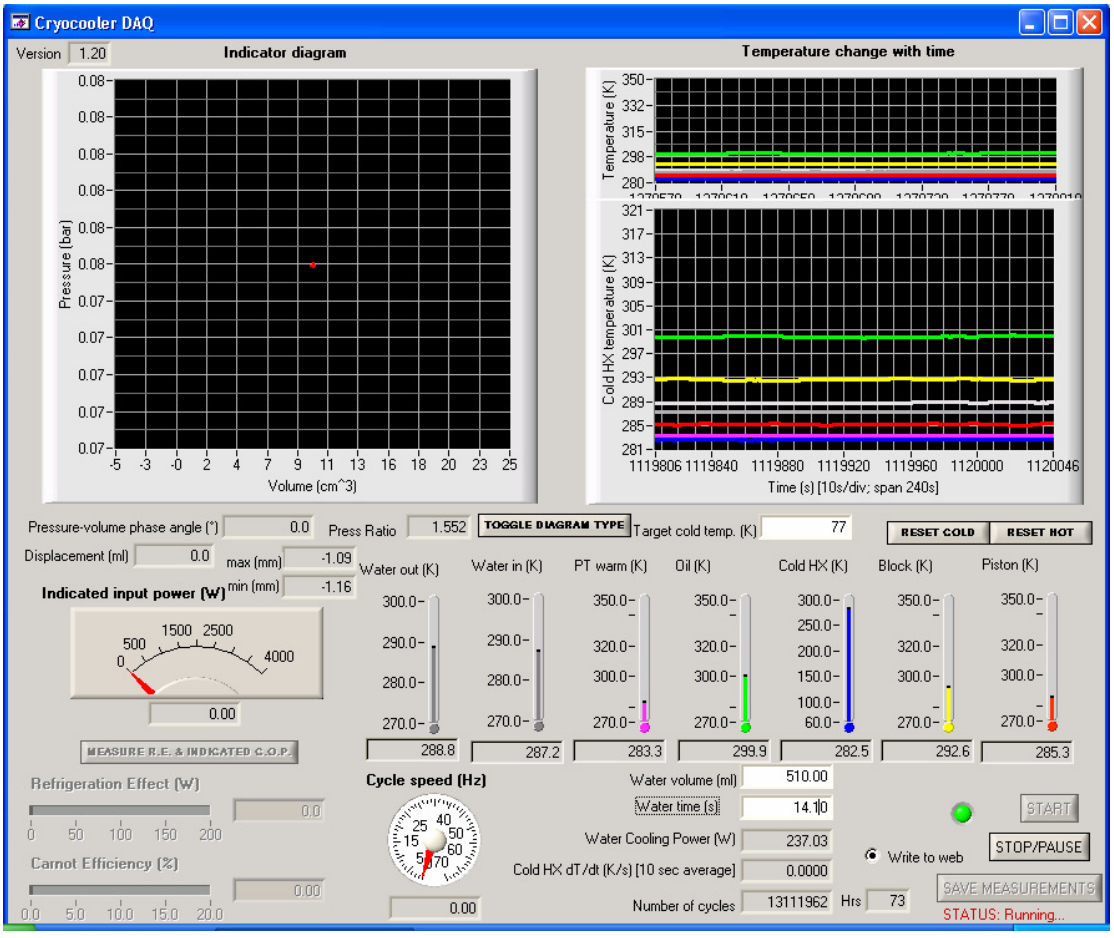

Figure 6.8. Data acquisition interface

6.2.5 Cooling Power

Two different approaches were used to determine the cooling power achieved by the pulse tube. The first method was a transient approach in which the cool-down rate of the copper block of the cold head heat exchanger (the dominant thermal mass in the pulse tube) was recorded. The consequent analysis of this recording required a knowledge of the temperature dependence of the specific heat of copper over this temperature range, NIST data[18] was used for this purpose.

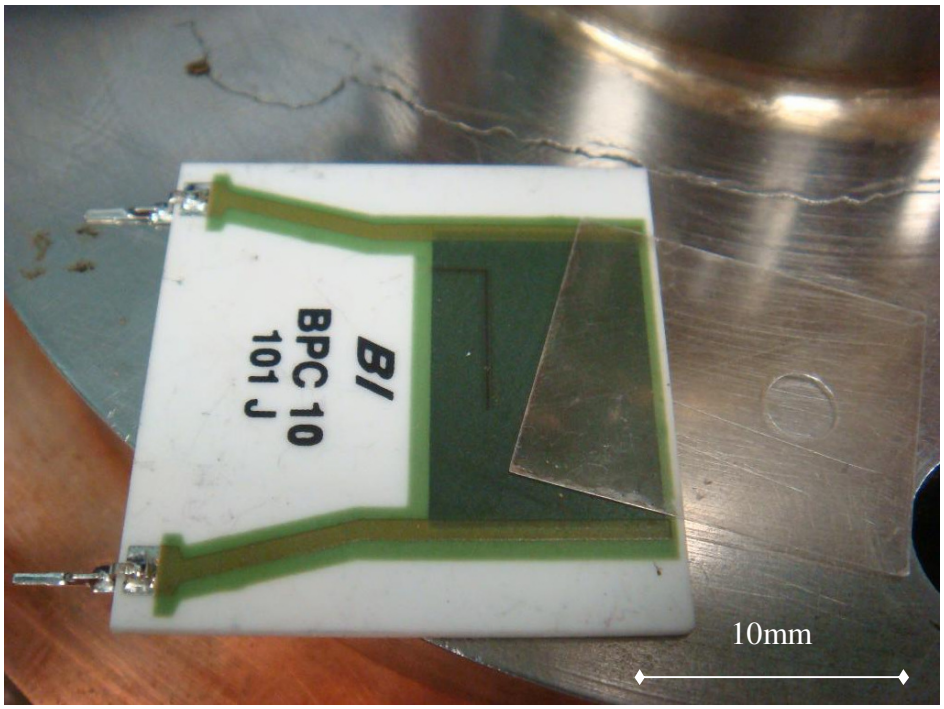

Figure 6.9. Resistive heater for power measurements

The second approach to the determination of the cooling power was to apply a steady heat with four ceramic flat type 10 W / 100 Ω resistors (Figure 6.9), which were clamped to the cold-head. The power was measured, via a four-wire connection. The two methods agreed with each other to within 4 K over a 60 to 80 K range.

A 120 W power supply was used to supply a variable voltage and current to the heaters, as pictured in Figure 6.10. Obtaining exact values for the cooling power was difficult since the voltage and current were adjusted separately (they also affected each other) and had to be read off individual meters and multiplied. However, values were found which could be repeated between experiments, by maximising one channel and adjusting the other, for the purposes of relative comparisons.

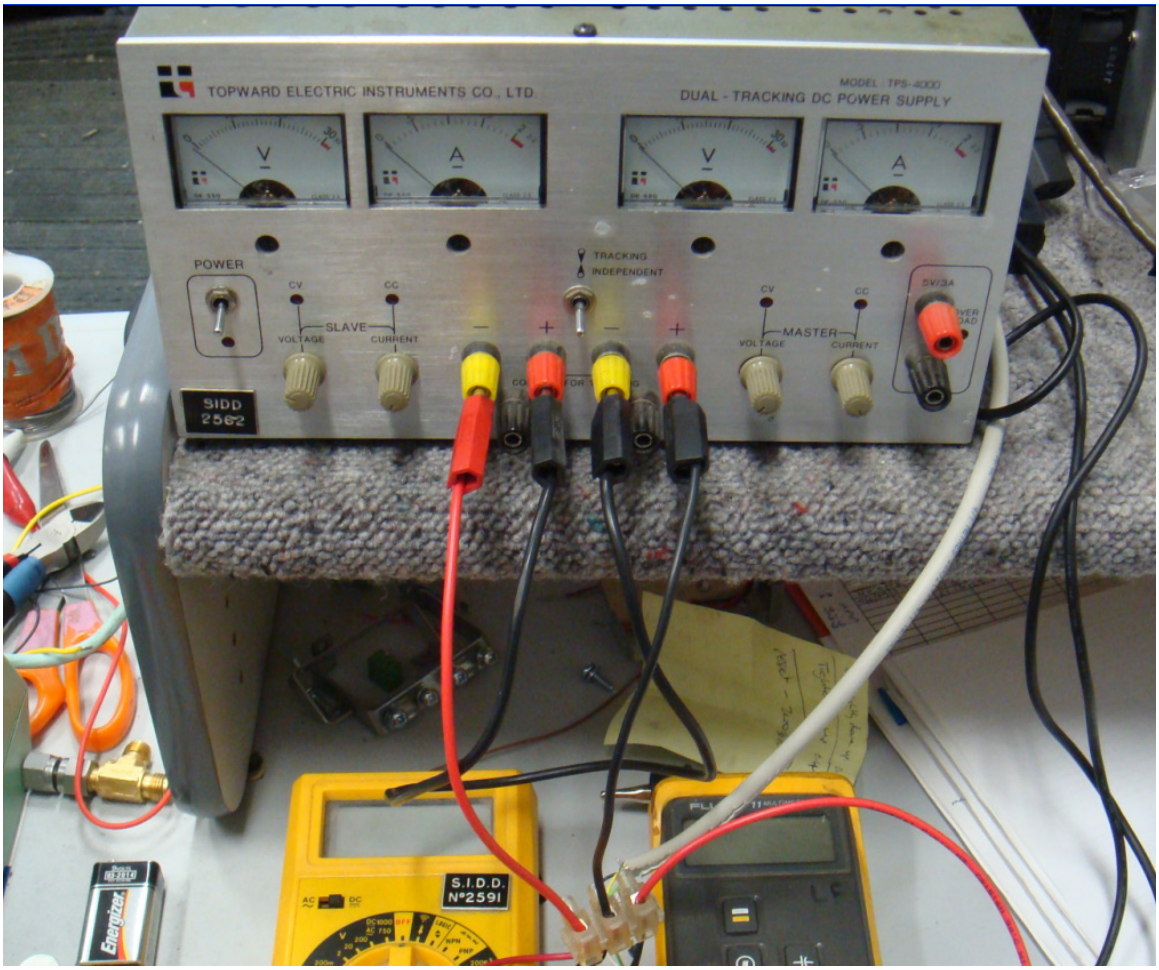

Figure 6.10. 120 W power supply and instruments for power measurements

6.3 Laboratory

6.3.1 Vacuum Pumps

The vacuum pumps were connected to the PT2050 pulse tube's cryostat through 50 mm diameter tubes, using flexible sections where appropriate. The vacuum pump arrangement is pictured in Figure 6.11. The roughing pump reduced the pressure in the cryostat to 10^{-3} millibar. A diffusion pump was then used in series with the roughing pump, which lowered the pressure to approximately 10^{-7} millibar. Technical grade helium was used as the working gas, which was supplied through lines to the reservoir, and had valves and connectors to isolate the gas bottle. The system was vacuum purged system overnight to outgas contaminants and to remove air.

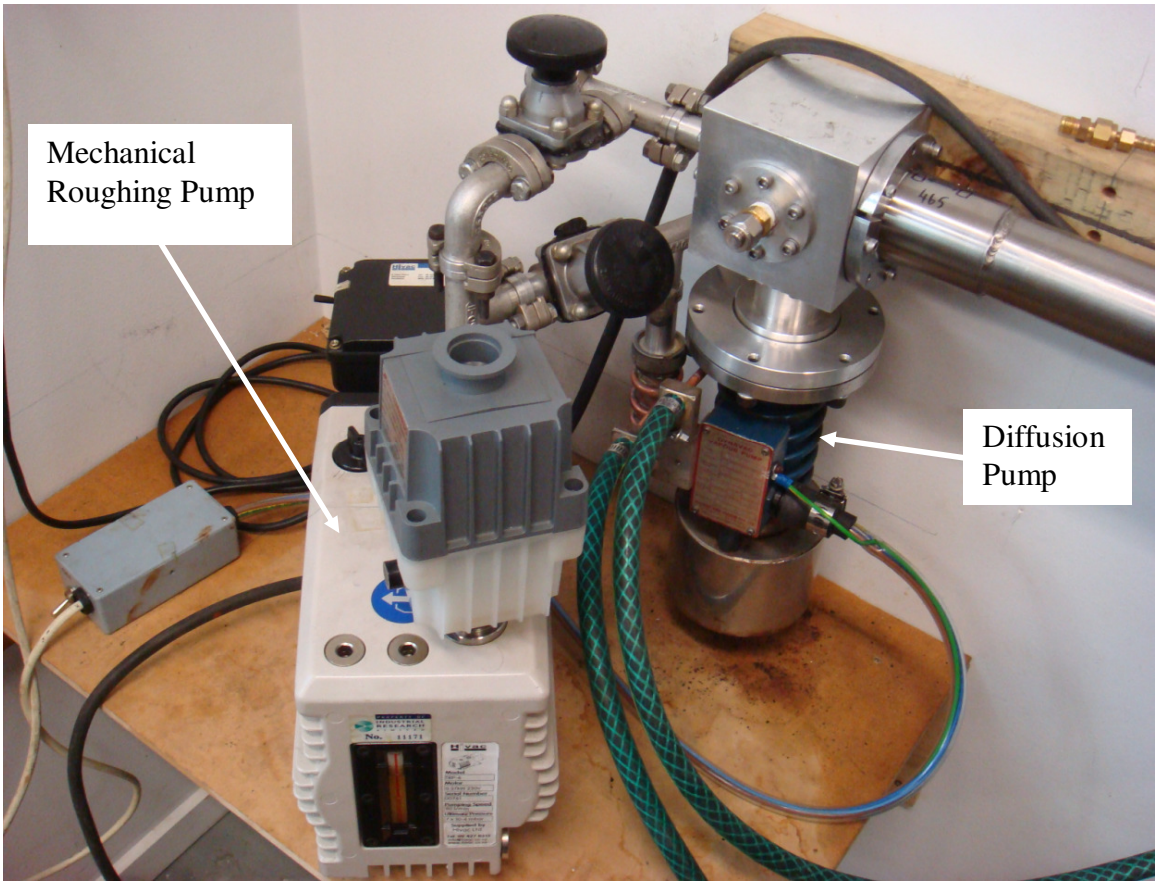

Figure 6.11. Photograph of the roughing and diffusion vacuum pumps

6.3.2 Vacuum Gauge

A Thyracont combination Pirani/Penning vacuum sensor VSM72MV (Figure 6.12) and gauge VD952 (Figure 6.13) were used to determine if an appropriate vacuum for the coldhead insulation was achieved. The sensor was fitted to a ported block about midway between the cryostat and the vacuum pumps. The reason for this was to enable the flexible line to be able to be used for many applications with the vacuum sensor permanently attached. The life of the sensor on the cryostat, which was subject to machine vibration, was another reason for the mounting position of the sensor.

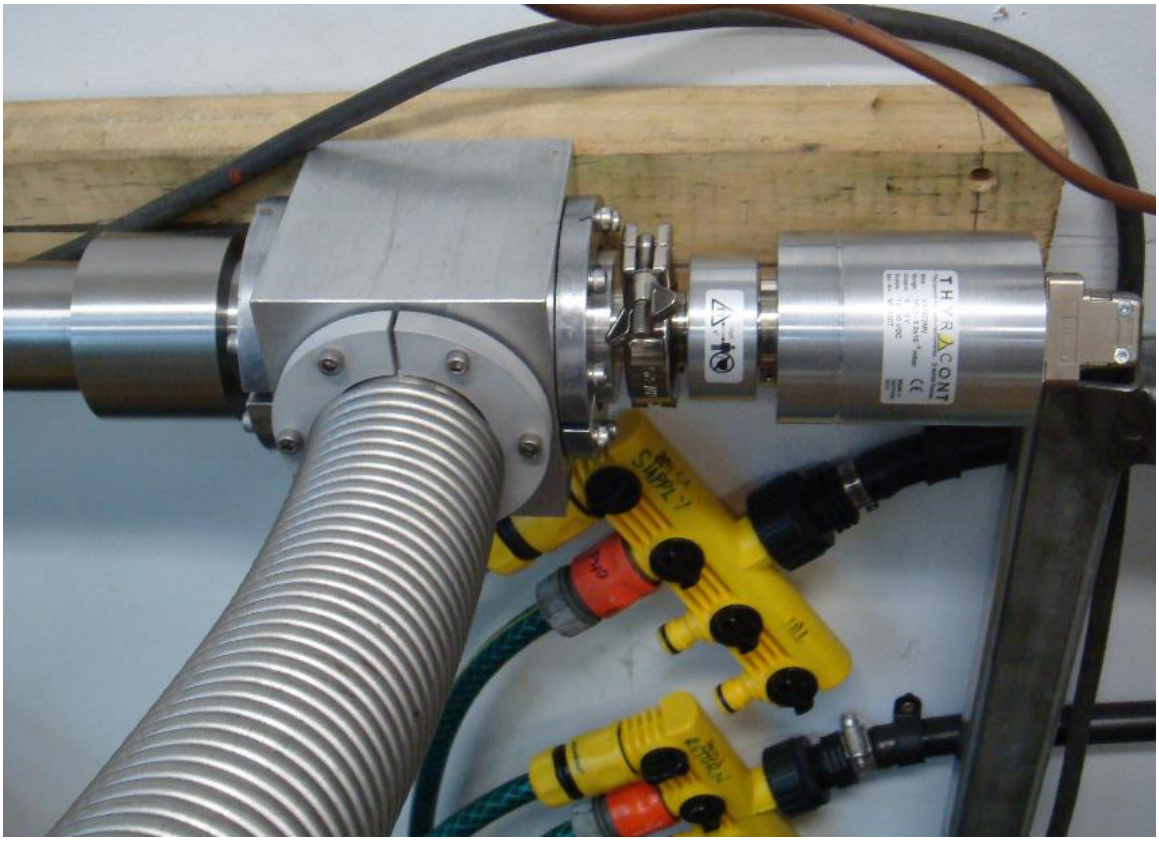

Figure 6.12. Photograph of the vacuum gauge

Figure 6.13. Photograph of the Lakeshore temperature monitor and vacuum gauge

6.3.3 Water Cooling

Cooling water was supplied to the pulse tube (warm and after-cooler heat exchangers), the diffusion vacuum pump, and the water to oil cooler for the PWG by the use of fan cooled automotive radiators and a swimming pool pump. (For the on-going development of the pulse tube, this set-up will be replaced by an accurate chiller, which has recently been purchased to enable better control of the coolant temperature.)

6.3.4 Speed Control

The PWG speed was controlled by a 3-phase motor drive speed controller (ACS550-01-015A-4). An output panel displayed variables such as electrical drive frequency, a calculated motor output power, current, etc and allowed remote control of the drive frequency.

6.3.5 Experimental Set-up

The pulse tube was assembled and attached to the CHC60 PWG. Testing was carried out in-house at IRL in Christchurch. An experimental facility was set up with the data acquisition, vacuum pumps, speed control for the drive motor, water cooling, helium supply and appropriate working areas. Figures 6.14 and 6.15 show the laboratory set-up with labels describing various associated components.

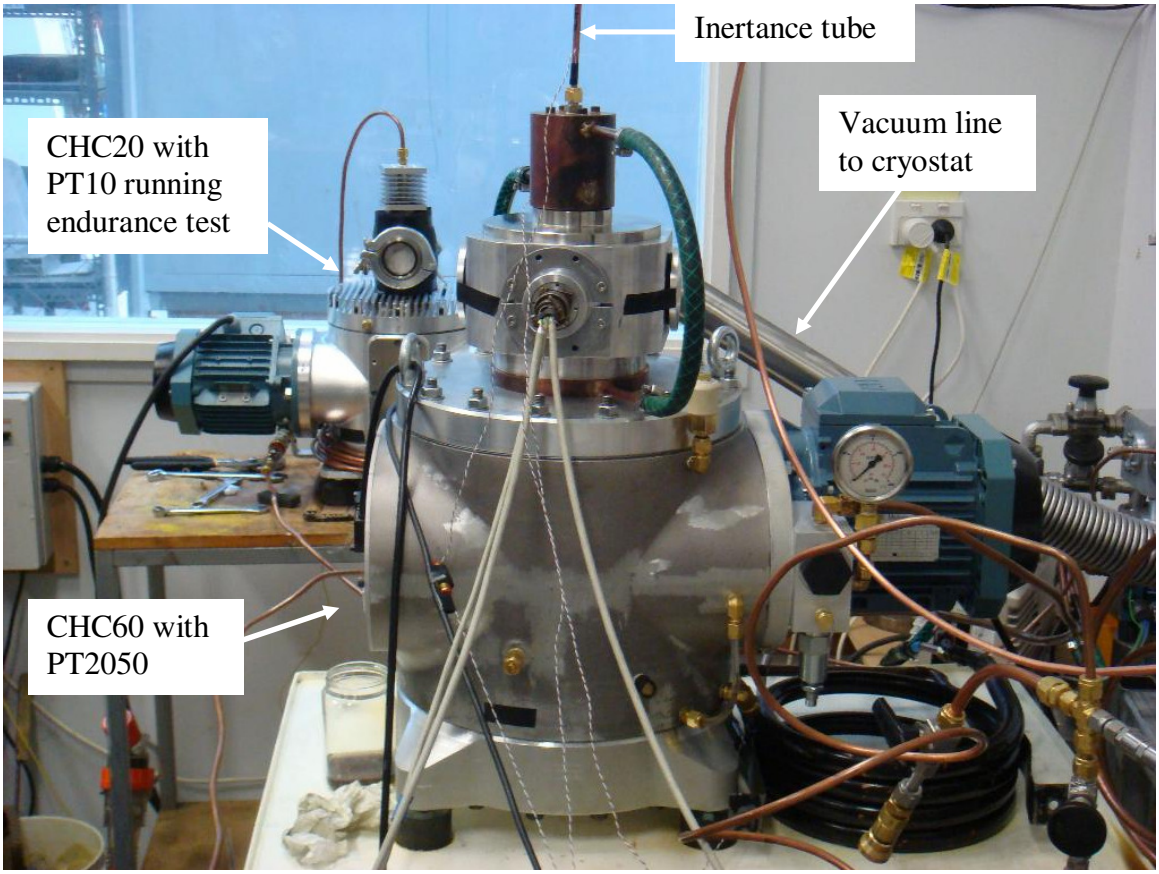

Figure 6.14. Photograph of the experimental set-up

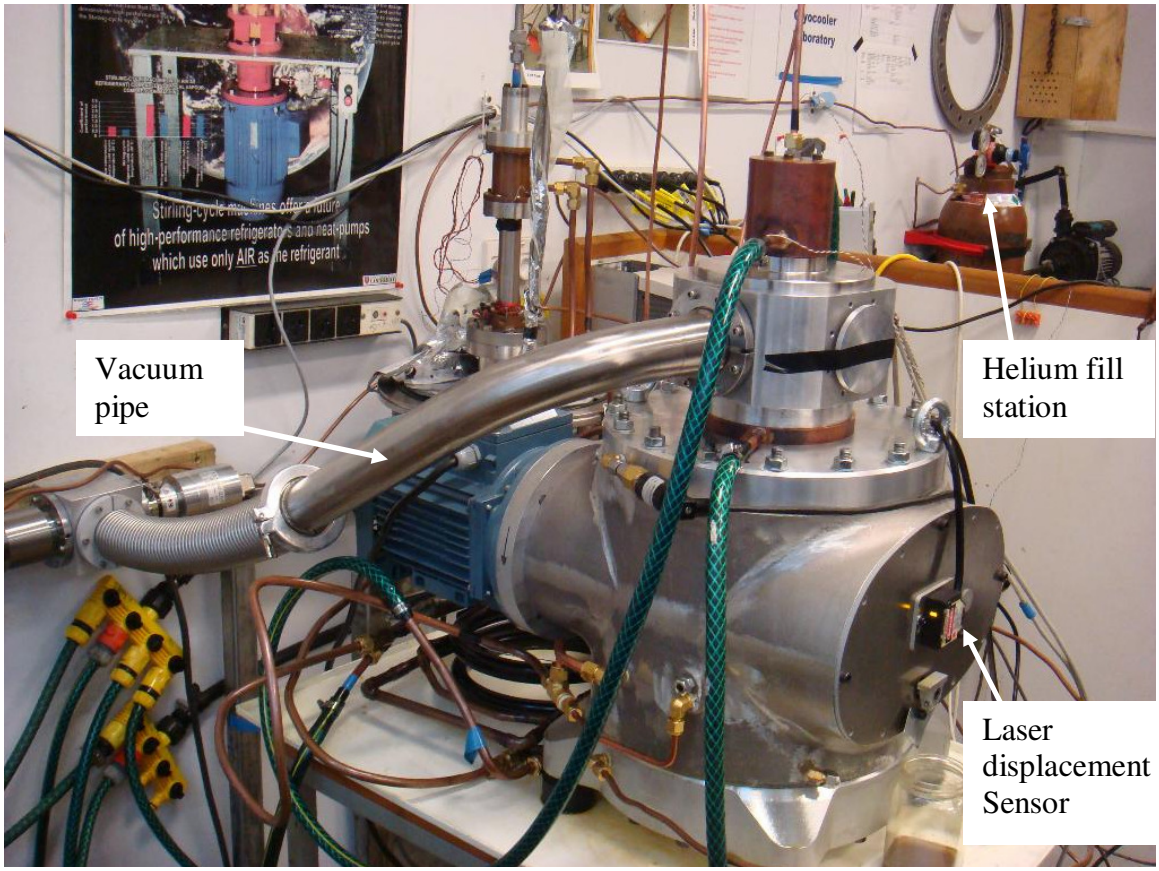

Figure 6.15. Laboratory set-up of the PT2050 closely coupled to the CHC60 PWG

7 Experimental Results and Comparison with Sage

7.1 Test Planning

The tests were planned around the fundamental tuning parameters of a pulse tube. Some initial testing and characterisation was carried out on a large 240 cc PWG, and also an orifice valve phase shifter replaced the inertance tube for testing the pulse tube at the early stages of running on the 60 cc PWG.

There are many parameters that could have been tested, but it was decided to test two main control parameters to establish a characteristic set of results to compare to the Sage model. The parameters chosen to be varied individually under test conditions with an inertance tube and reservoir were the mean gas pressure and the frequency of the pressure wave. Once the inertance tube and the reservoir were fitted to the PT2050 on the CHC60 PWG it was decided to test several frequencies and two mean gas pressures. Initial testing suggested that the designed performance of 20 W @ 50 K was not going to be achieved, so it was decided to conduct experiments which allowed cooling power results to be obtained at 77 K (the temperature at which nitrogen liquefies).

A test matrix, Table 7.1, was drawn up to enable efficient use of test time. The frequency range used to obtain the results was determined during testing. At first the frequency that gave the lowest no-load temperature was run, and power levels were set to find out the steady state temperature for the given frequency. This was only a starting point, as the frequency did not always compare well with the optimum frequency to produce the highest cooling power at 77 K. Values on either side of this frequency were then tested until a result was obtained on either side of a peak value for the cooling power at 77 K.

Table 7.1. Matrix of test parameters

Test #	Frequency	Pressure
	Hz	bar
1	42	25
2	44	25
3	46	25
4	42	15
5	44	15
6	46	15

Ultimately this intended frequency range was increased to 33-46 Hz to allow a more complete comparison to the Sage model. The higher frequency runs above 42 Hz were not conducted for the higher gas pressure runs as it was discovered that the PWG stroke decreased at the higher mean gas pressure, possibly due to internal leakage in the prototype hydraulic amplifier system. Sage predicted that the decreased stroke would cause a loss of performance in terms of cooling power, and this could explain in part why there was not the improved performance indicated by Sage at the higher mean gas pressures.

Other parameters were held as close to constant as possible. A reservoir size of 2.3 litres and an inertance tube length of 4 m and internal diameter of 4.3 mm were chosen to conduct the experiments. The optimised Sage prediction was for a 2 m inertance tube, but the experimental result, after changing the inertance tube to 4 m during some initial testing, was that the 4 m provided better cooling performance.

Some of the potential noise factors (parameters which can drift and are not controlled implicitly) include, but are not limited to, the following: PWG piston drift (dead volume), PWG piston stroke, coolant temperature, ambient temperature, vacuum insulation, helium gas purity, etc. These factors add to create non-repeatability in the experiments.

7.2 Thermal Leakages

7.2.1 Experimental Measurements

The total parasitic heat leak in a pulse tube is the summation of conductive and radiation heat leaks. The summation of these heat leaks can be deduced from the rate of temperature rise, at the temperature of interest, when the pulse tube is turned off after operation. In these circumstances the enthalpy/entropy losses due to the gas movement within the pulse tube are not included. The deduced leaks are attributable to effects such as: working gas conduction, regenerator mesh conduction, pulse tube conduction, regenerator tube conduction, sensor wire conduction, heater wire conduction, cryostat radiation, cryostat gas conduction, cryo-pumping and MLI conduction and radiation leaks.

The heat leak was measured using a procedure[5] that involved measuring the warm-up rate at a set temperature with a range of heat loads applied to the cold-head. Extrapolation back to a zero warm-up rate gives the heat leak into the cold-head. The heat-up rate, in Kelvin per second, was recorded for each of the three powers in separate runs at 80, 90 and 100 K, and then plotted as is shown in Figure 7.3. All three temperatures exhibited a thermal heat leak of just under 10 W with the highest loss at the lowest cold temperature, as would be expected.

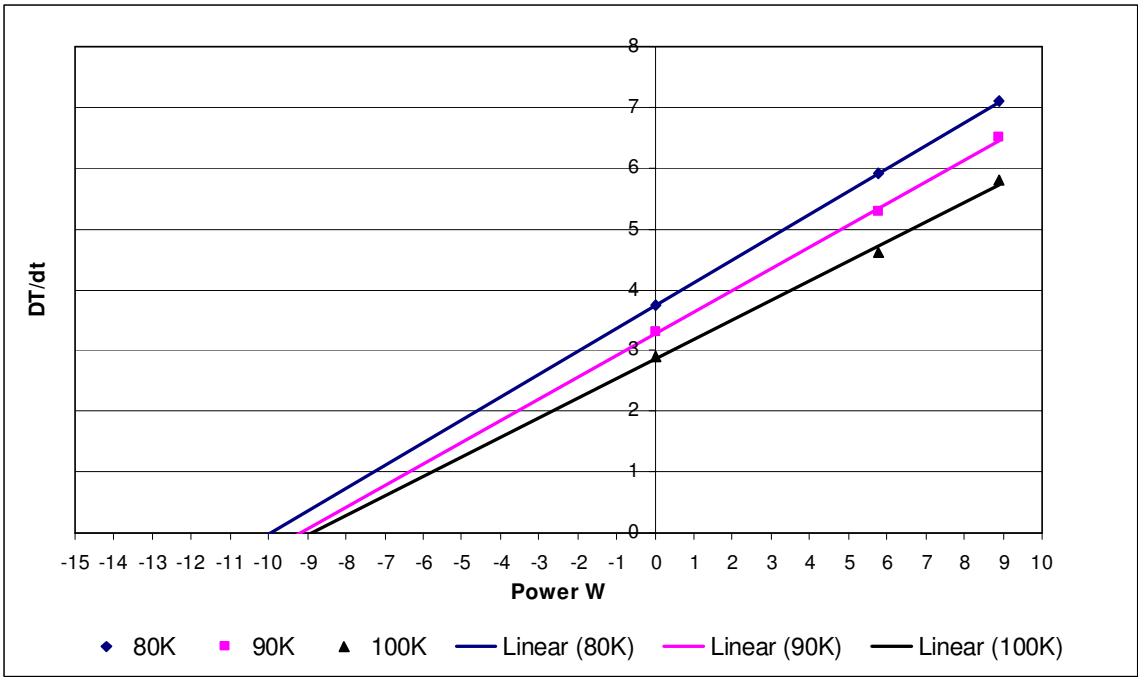

Figure 7.3. PT2050 thermal base loads at 80, 90 and 100 K with 2 x 10^{-7} mbar vacuum and MLI

7.2.2 Estimated Thermal Leakages

Some of the thermal leakages such as radiation in the cryostat and conduction in the pulse and regenerator tubes, and conduction down the sensor and heater wires have been estimated using basic thermodynamic principles, and are summarised in Table 7.2. Appendix A shows the tube calculations.

Table 7.2. Calculated thermal leakages

Radiation - Cryostat	3.3 W without MLI
Conduction - Regenerator tube	1.9 W
Conduction - Pulse tube	0.6 W
Conduction - Wires	0.2 W

7.2.3 Leakages and Losses not included in the Sage Model

The Sage model did not include some of the parasitic heat leaks such as thermal insulation within the cryostat, but did include the regenerator and pulse tube conductive leaks. Other various 3D flow effects have also not been quantified in the PT2050:

- Acoustic streaming in the pulse tube, which involves circulating flow losses, can occur in high frequency pulse tubes of this size[19]
- Secondary flows (also a circulating flow loss) in the regenerator can also occur in high frequency pulse tubes[20]
- Flow straightener losses due to the pressure drop associated with straightening the flow in the pulse tube
- An unaccounted pressure loss exists in the PWG as the compression p-V work is calculated without the effect of the gas changing direction 90° to go into the pulse tube. A Computation Fluid Dynamics (CFD) analysis has been conducted, in a separate project at IRL, to determine the significance of these losses and to find a solution.

7.3 Initial Testing

7.3.1 CHC240 PWG

As has been mentioned already, initially the pulse tube was run on a 240 cc swept volume PWG as the 60 cc PWG was not available. A buffer volume was inserted between the PWG[3] and the pulse tube to reduce the pressure ratio. Even so, a low charge pressure of 0.9 MPa was necessary to limit the magnitude of the pressure wave and to avoid damage to the PWG drive. The lowest no-load temperature of the pulse tube on the 240 cc PWG was 49.6 K. The 0.9 MPa mean gas pressure resulted in a pressure ratio of 1.9. The optimum experimental frequency was 42 Hz with a 4 m inertance tube. 100 W of cooling power was produced at 105 K with 2.0 MPa mean gas pressure. From here on the testing was carried out on the CHC60 PWG.

7.3.2 Orifice Valve Phase Shifter

A 9.5 mm diameter orifice valve (ball valve) was used as the variable phase shifter, as a starting point in characterizing the performance of the pulse tube on the CHC60 PWG. Unlike using a fixed-length inertance tube, this testing enabled the phase shifter to be tuned to each frequency so that some understanding of the coldest temperature versus frequency map could be determined.

The orifice valve was placed after the transition cone at the warm end of the pulse tube and a 2 m long 9.5 mm diameter inertance tube was placed between the orifice valve and the reservoir. Frequencies of 40, 50 and 60 Hz were run with no-load temperatures and 25 W temperatures, with the results listed in Table 7.3. The valve opening was adjusted, to optimize the cold temperature, for each change in parameter. The best no-load frequency was the highest run frequency of 60 Hz with this phase shifter and average gas pressure. Further testing at higher frequencies was not conducted due to PWG motor limitations. With these preliminary orifice valve tests completed, all subsequent testing was conducted with a fixed-length inertance tube of 4 m.

Table 7.3. Orifice valve performance

Frequency	Avg. Pressure	Pressure ratio	Input p-V	p-V angle	Load	Warm Temp.	Cold Temp.
Hz	MPa		W	Degrees	W	K	K
40	2.612	1.377	767	149.6	25	290	103.2
50	2.621	1.387	1001	149.2	0	290	88.5
50	2.623	1.395	948	151.4	25	290	102.6
60	2.619	1.413	1254	148.0	0	290	87.6
60	2.620	1.414	1181	149.9	25	290	99.5

7.3.3 Cool-down

A typical cool-down curve showing the time taken for the PT2050/CHC60 cryocooler to reach a temperature is plotted in Figure 7.4. The cool-down was found to take about 15 minutes to cool to within 10% of the no-load temperature, and then a further time period of at least 12 hours to reach a true steady-state condition. The cool-down shown was run with 4 m inertance tube, 1.5 MPa mean gas pressure and at 40 Hz.

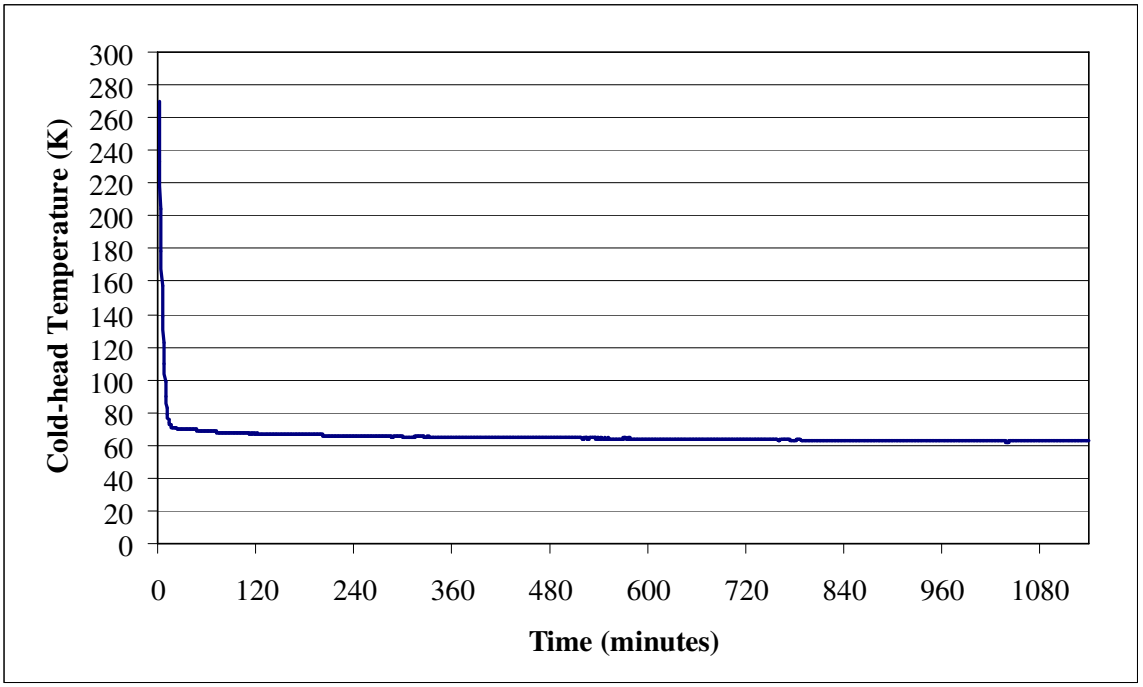

Figure 7.4. Cold-head temperature versus time plot

The machine was run down to a "no-load" temperature, where only the thermal leakages exist as a load. Once the steady state conditions were reached testing could be established. The resistive heaters were then used to provide a load, and measurement results were recorded once the machine reached steady state operation. Each power run took about an hour to reach steady state.

7.4 Sage and Experimental Results Compared

7.4.1 Frequency of Pressure Wave

One of the big advantages of the PWG used for the experiments was that the frequency of operation could be adjusted over a wide range. Figure 7.5 shows that there was a difference in the frequency, of about 7 Hz, to achieve optimum cooling performance between the Sage model and the experiment. A sensitivity analysis of the frequency was carried out in the Sage model that showed great sensitivity to inertance tube diameter – an 0.3 mm decrease in the measured 4.3 mm internal inertance tube diameter yielded a 4 Hz decrease in the optimum cooling power frequency. No appreciable optimum frequency change was found with changes to the dead volume in the compression space. A close to 1 Hz decrease in frequency is shown in Figure 7.5 when the mean gas pressure is dropped from 2.5 to 1.5 MPa. The experimental data for the 2.5 MPa run was not completed due to the PWG loss in displacement with the higher gas pressure.

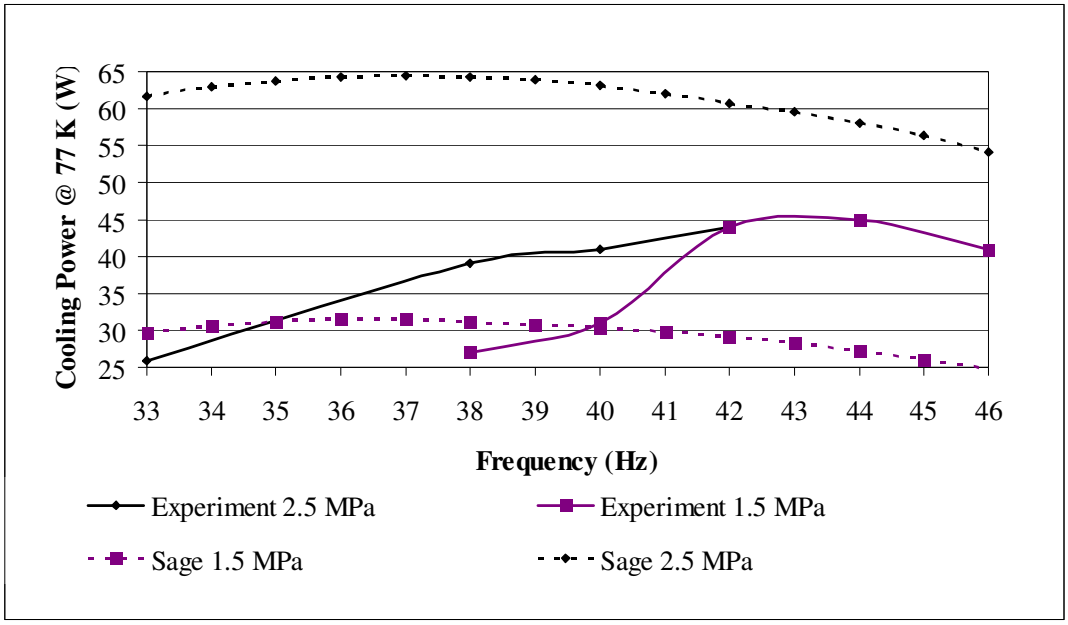

Figure 7.5. Frequency sweep versus cooling power @ 77 K

The comparisons from here on were conducted at the optimum experimental frequencies, since frequency is shown to have a more significant effect on cooling performance at 77 K in the experiments.

7.4.2 Pressure Ratio

The pressure ratio is the ratio of the maximum and minimum pressures in the compression space. The effect of the frequency of the pressure wave on the pressure ratio is shown in Figure 7.6 for the 1.5 MPa and also the 2.5 MPa mean gas pressures. The pressure ratios in the experiments are shown to be greater than the Sage model for a given temperature. There are several variables that contribute to the pressure ratio, such as: dead volume in the compression space (geometric), PWG displacement (dynamic), pressure drops through the pulse tube system (fluid flows) and also how effectively the gas is cooled (thermodynamic). Table 7.2 shows the pressure drop and phasing of the pressure waves at both ends of the pulse tube and at the reservoir.

Both Sage and the experiments are in agreement in showing that the pressure ratio is lower for the greater mean gas pressure. There is a greater difference between the two experimental results than there is between the Sage results. This could be attributed to the higher pressure run not achieving the same PWG displacement as the lower pressure run.

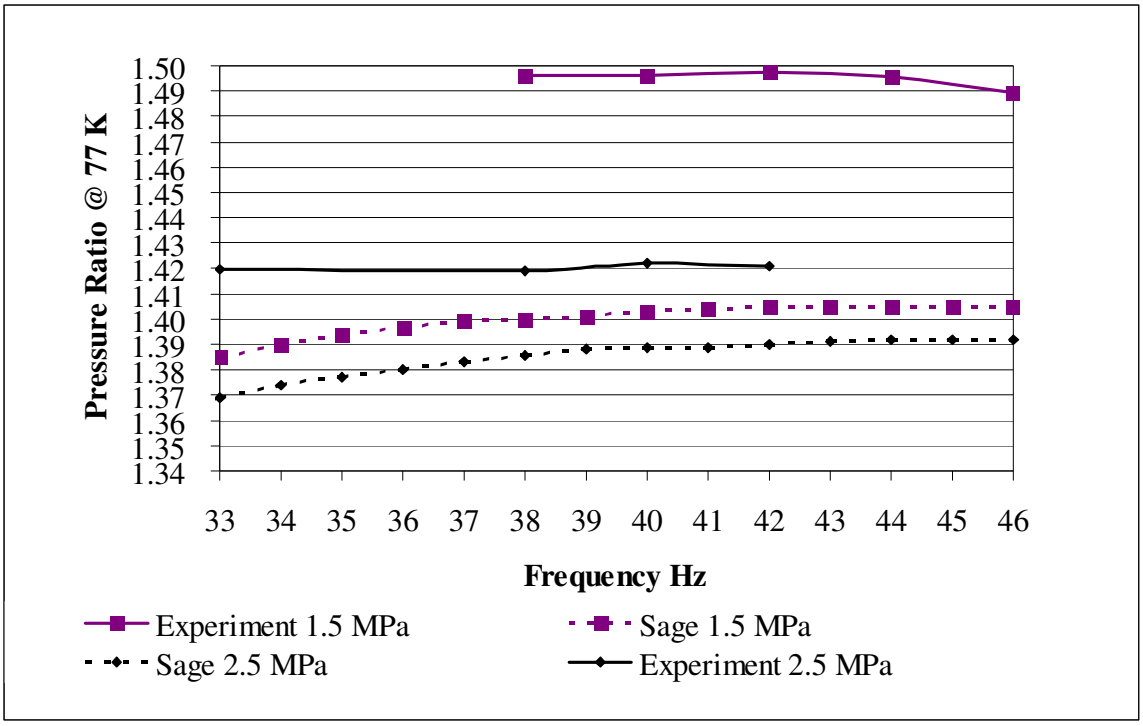

Figure 7.6. Pressure ratio versus frequency

7.4.3 Working Gas Pressure – Volume Phasing

p-V Phase in the Compression Space

The phase angle between the compression space pressure and the volume has been plotted in Figure 7.7. This is another valuable comparison, which can give information as to whether the pulse tube is operating correctly. The phase difference occurs due to the same factors as described for the pressure ratio. Again the lower displacement and the non-optimal PWG frequency of the 2.5 MPa run would contribute to the lower phase angle shown. The 1.5 MPa runs are fairly similar between the Sage model and the experiment.

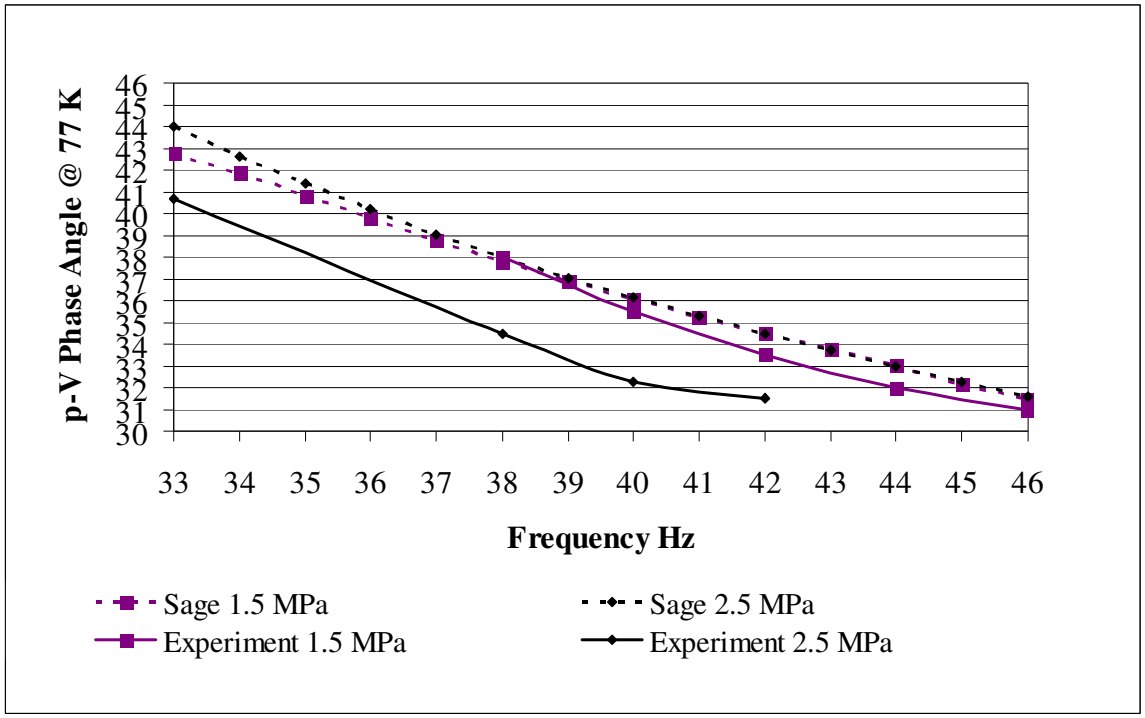

Figure 7.7. p-V phase angle in compression space versus frequency

Gas Phasing across the Inertance tube

As a further analysis tool in correlating the Sage model to the experimental data an experiment was conducted to determine pressure drops and phase relationships through the pulse tube. Three pressure gauges were connected to either end of the inertance tube - one at the reservoir end and one at the warm end of the pulse tube, and one in the compression space as was shown in Figure 7.7.

The resulting amplitude and argument are presented in Table 7.4 along with the Sage outputs for the same positions. The argument is the phase relationship between the pressure measurement at each of the three positions and the compression space volume. The experiments were conducted with a 4 m inertance tube, 2.5 MPa mean gas pressure, 42 Hz pressure wave and at 77 K cold temperature. A similar trend can be seen between the Sage and experimental results: the amplitudes decreased as the measurement point was further from the PWG; phasing was greatest at the warm end. The experimental results show higher amplitudes, which could be due to many factors, as discussed in Section 7.4.3.

Table 7.4. Pressure amplitude and phase – Sage and experimental results

	Sage		Experiment	
	Amplitude	Argument	Amplitude	Argument
Compressor	3.96	-147	4.32	-149
Warm End	2.95	-156	3.21	-163
Reservoir	0.08	-132	0.14	-113

7.4.4 Input p-V Power

The p-V input power is shown in Figure 7.8 plotted against the cold-head temperature. Both the experimental and the Sage results predict that as the mean gas pressure is increased, more p-V input power is required to drive the cryocooler. There is a larger difference between the Sage results than there is between the experimental results, which could be a result of the lower displacement in the PWG at the higher mean gas pressures. The higher pressure run also was conducted at 42 Hz where the optimum frequency was higher, so this would also produce a lower p-V power.

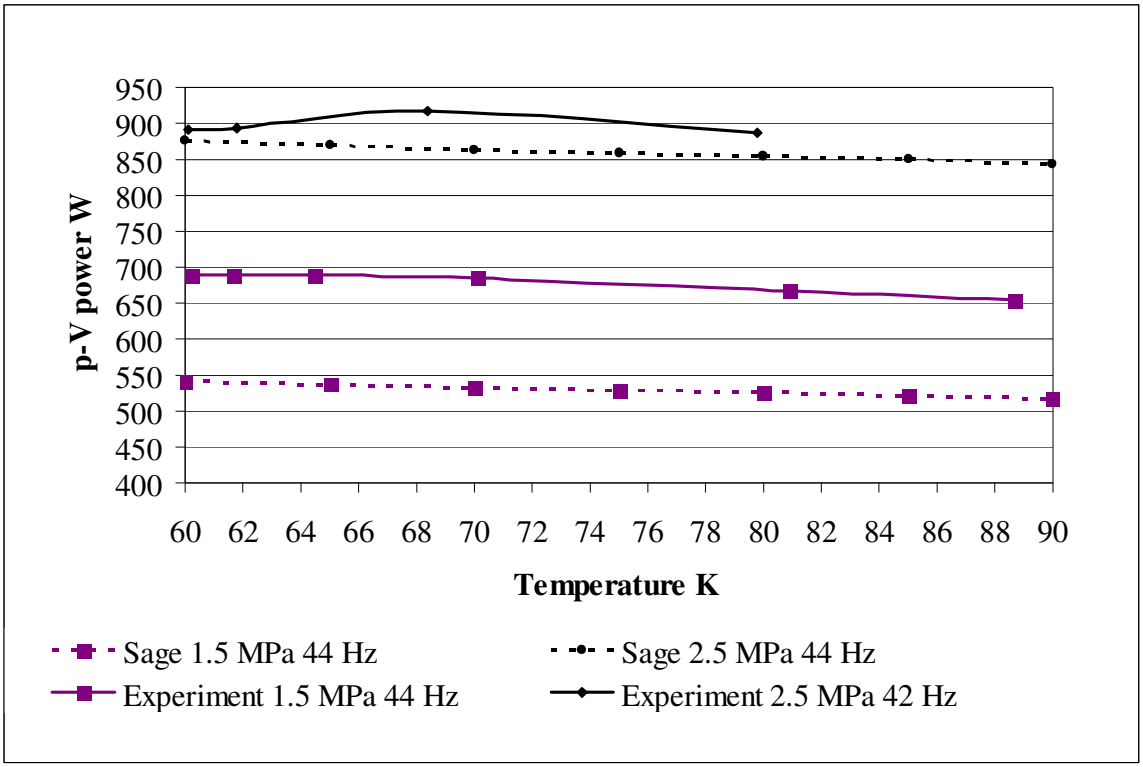

Figure 7.8. p-V input power versus cold temperature

7.4.5 Cooling Power

Figure 7.9 shows the cooling power achieved for both the Sage model and the experiment. Two gas pressures (1.5 MPa and 2.5 MPa) were run and plotted. The experimental performance at the higher temperatures shows promise, but the higher gas pressure run was at a non-optimal frequency and had a reduced PWG displacement. Possibly greater that predicted cooling power at 77 K shown in Figure 7.9 could be explained by the higher pressure ratio of the experimental 1.5 MPa run compared to Sage (Figure 7.6).

The drop in performance in the experiment relative to the Sage model as the temperature is reduced may be due to thermal and fluid 3D effects in the pulse tube, which were not modelled in Sage.

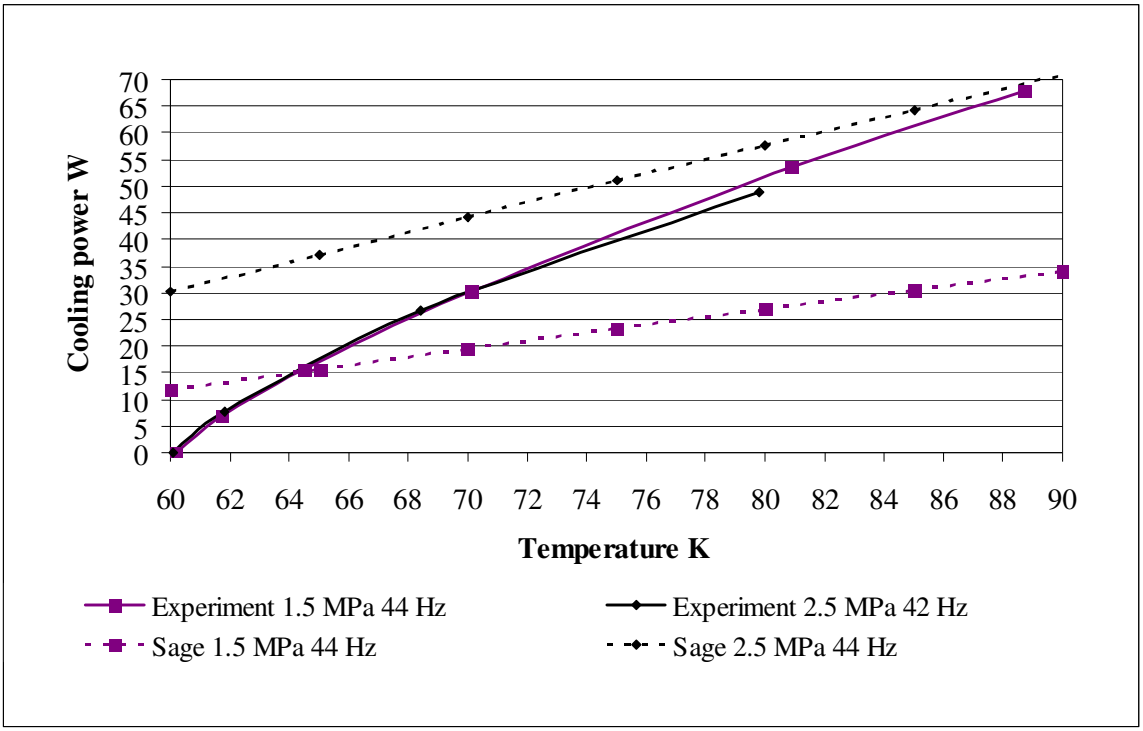

Figure 7.9. Cooling power versus cold temperature

7.4.6 Percentage of Carnot Coefficient of Performance

A comparative measure of the Carnot coefficient of performance (COP) based on p-V input power, refrigeration power, and cold and warm temperatures has been carried out, and is presented in Figure 7.10. The Carnot COP shown is the percentage of the Carnot COP that was achieved by the PT2050 under the conditions shown in the legend of the graph. The COP is displayed against cold-temperature, which has a significant effect on the COP. Again the experiment shows a reduced COP that Sage does not predict as the lower temperatures are achieved.

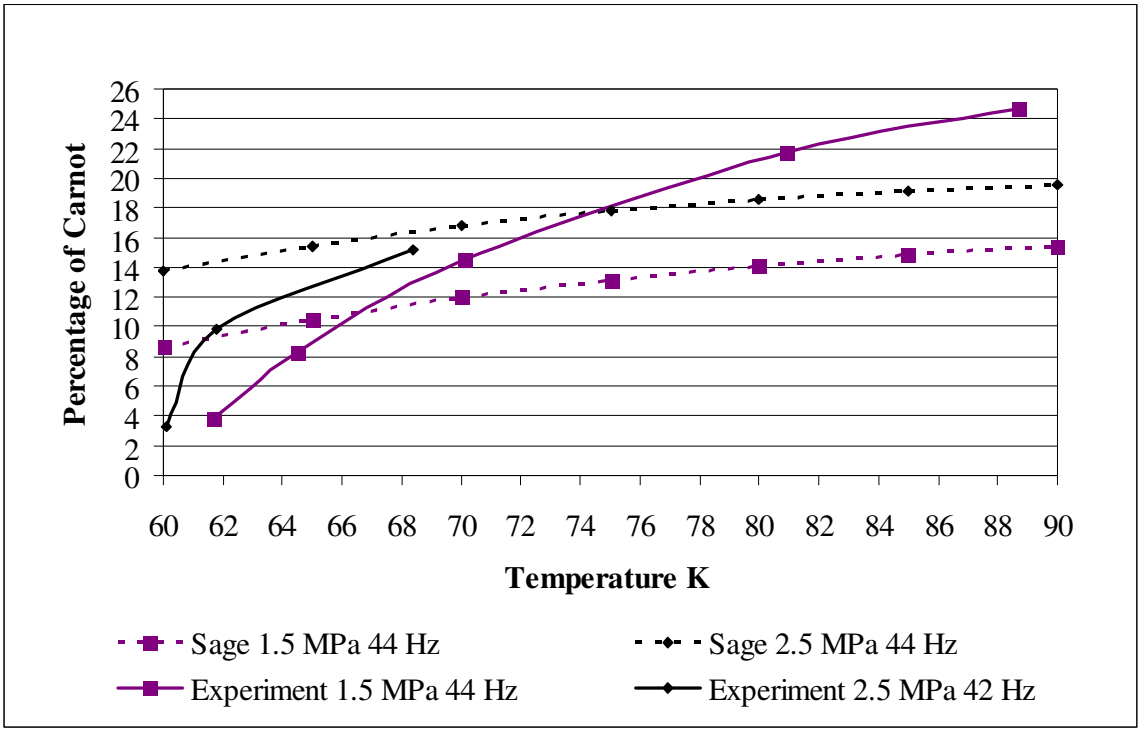

Figure 7.10. Percentage of Carnot COP versus cold temperature

8 Conclusions and Recommendations

8.1 Conclusions

Sage software was used as a tool to thermodynamically design the PT2050 pulse tube coupled to the CHC60 PWG. A model was constructed which included the geometries, movements, fluid flows and thermodynamics of the cooler. The pulse tube was designed and fabricated. Throughout the course of this development work the Sage model had refinements and improvements made, both in modelling technique and in response to changes to components and features during the manufacture and assembly of the pulse tube and PWG. The updated model, with a 2 m inertance tube and 2.5 MPa gas pressure, predicts cooling power to be 35 W @ 50 K as compared to the original prediction of 25 W @ 50 K.

Initially the pulse tube was coupled to a CHC240 PWG. A buffer volume was inserted between the pulse tube and the PWG to reduce the pressure ratio entering the pulse tube, which was limited by the PWG. A lowest no-load temperature of 49.6 K with 0.9 MPa gas pressure and 50 W of cooling power at 77 K with 2.0 MPa gas pressure was achieved. Testing on the 240 cc PWG indicated that higher mean gas pressure gave greater cooling power, with the downside of higher no-load temperatures.

On the smaller CHC60 PWG it was found that a 4 m long inertance tube was more optimal than the 2 m long inertance tube predicted by the Sage model. A lowest no-load temperature of 55 K and 46 W of cooling power at 77 K were achieved with a 44 Hz pressure wave frequency (46 Hz electrical input frequency), 1.5 MPa mean gas pressure and the 4 m long inertance tube. A corresponding Carnot COP of 19.5%, based on the p-V input power of 675 W, was also achieved. The 77 K values were used since the pulse tube did not reach the desired temperature of 50 K, and the development was split into two parts: creating power at 77 K and reducing the lowest no-load temperature. The refined Sage model predicts 25 W and 55 W of cooling at 77 K and a Carnot COP of 13% and 18%, for the respective 1.5 and 2.5 MPa mean gas pressures. The under prediction

on the cooling power by Sage for the 1.5 MPa comparison with the experiment could be explained by the greater than predicted pressure ratio.

The significance of the two parameters (frequency and mean gas pressure) were compared between Sage and the experiment. The higher mean gas pressure of 2.5 MPa created a higher pressure amplitude than the 1.5 MPa pressure. It was found that the higher pressure amplitude led to a reduced stroke, and therefore displacement, from the PWG. The 2.5 MPa experiments did not achieve the Sage predicted improvements over the 1.5 MPa runs. This could have been attributed, at least in part, to a reduced stroke in the PWG at the higher pressure.

At the lower temperatures the experiments tailed off quite rapidly to a higher temperature than the Sage model predicted. With this size of pulse tube it has been documented[19, 20] that several 3D effects can occur, which limit the reduction in temperature. Personal communications with Jim Maguire (AMSC) and David Gedeon (Sage) have supported the view that 3D effects would need to be considered in the quest to achieve lower temperature performance.

An overall concluding summary of the most significant achievements and finding of this work would be:

- Although by no means perfect, some correlation has been found between the Sage model and the experimental results.
- In retrospect the target of 20 W at 50 K was a fairly ambitious one for a first attempt at producing usable cooling power from a pulse tube.
- A loss of displacement from the PWG at higher gas pressures, plus the distinct possibility of power robbing 3D effects within the pulse tube itself may have contributed to some of the differences between the predicted and achieved cooling performances.
- Despite these deficiencies that were not allowed for in the Sage model, a lowest no-load temperature of 55 K and 46 W of cooling power at 77 K were achieved, with corresponding Carnot COP of 19.5%, based on p-V input power.

- Although not an accurate representation of the actual pulse tube performance, the Sage modeling proved to be an invaluable tool during the design process.

Work is continuing on trying to gain a fuller understanding of the differences between the Sage model and the experiment in order to more efficiently design PWG – pulse tube cryocoolers. This project has provided a good basis for further development of pulse tubes at IRL.

8.2 Recommendations for Further Work

Many development opportunities have arisen from the work carried out in this thesis. The most important of these are outlined below:

- Develop the PWG to provide a more consistent stroke with varying loads. The aim is to reduce the leakages from the hydraulic actuation system, since it is believed that the leakages could be greater than required. A short term solution is to run lower mean gas pressures.
- Find the optimum inertance tube length and diameter by experimentally mapping the geometry with frequency.
- Develop the low temperature performance of the pulse tube to achieve cooling power in the 30 – 50 K temperature range:
    - Reduce some of the known 3D fluid losses and thermal leakages characteristic of this size of PTR:
        - A CFD – Sage analysis of the pulse tube should be carried out, and if possible verified experimentally.
        - A length/diameter ratio of pulse and regenerator tubes should be experimentally mapped to find an optimum cooling performance
        - A tapered pulse tube[19] should be tested to compare its affect on cooling power and temperature
        - An experimental optimisation of the flow straightener mesh size would be useful

- Design and develop a multi-stage pulse tube, which allows colder temperatures to be reached, with a higher temperature cold-head to lift heat at a higher temperature.

- Develop a more practical pulse tube design
  - Co-axial pulse tube, which has a cold-head at the extreme end of the cooler for better accessibility.

References

1. Caughley, A.J. et al, "A Low Cost Pressure Wave Generator using Diaphragms", *Advances in Cryogenic Engineering,* Volume 53B, p1122-1129.
2. Caughley, A.J. et al, "Diaphragm Pressure Wave Generator Developments at Industrial Research Ltd", *Advances in Cryogenic Engineering*, Volume 55.
3. Radebaugh, R., Foundation of Cryocoolers Short Course (2010), International Cryocooler Conference 16.
4. Carnot, S., "Reflections on the Motive Power of Fire" (1824).
5. Gifford, W.E. and Longsworth, R.C. (1963) "Pulse-tube refrigeration", ASME paper No. 63-WA-290 presented at Winter Annual Meeting of the American Society of Mechanical Engineers, Philadelphia, Pennsylvania
6. Mikulin, E.I., Tarasov, A.A. and Shkrebyonock (1984) "Low-temperature expansion pulse tubes", *Advances in Cryogenic Engineering 29*, Plenum Press, New York, p629
7. Matsubara Y, Miyake A. (1988) "Alternative methods of the orifice pulse tube refrigerator", *Proceedings of the 5th international cryocooler Conference*, p127 – 35
8. Zhu, S., Wu, P. and Chen, Z (1990) "Double inlet pulse tube refrigerators: an important improvement", *Cryogenics 30*, p514
9. Yang, L. W., Liang, J. T. and Zhou, Y. (1992) "Analysis and Experimental Research of a Multi-Bypass Version Pulse Tube Refrigerator", *7th International Cryocooler Conference*
10. Kanau, K., Watanabe, N., Kanazawa Y. (1994), "Miniature PTR for temp below 100 K", *Cryogenics 34*, p167 - 170
11. Hu J.Y., Luo E.C., Wu Z.H., Dai W. and Zhu S.L. (2007) "Investigation of an innovative method for DC flow suppression of double-inlet pulse tube coolers"
12. http://en.wikipedia.org/wiki/Helmholtz_resonance

13. Roach, P.R., Kashani, A., "Pulse Tube Coolers with an Inertance Tube: Theory, Modeling, and Practice", *Advances in Cryogenic Engineering, Vol 43,* (1988), p1895-1902.

14. Gedeon, D., *Sage 6 User's Guide*, Gedeon Associates (2009).

15. AMSC internal company report – unpublished, (2003)

16. Yuan, J., Maguire, J., "Development of a Single Stage Pulse Tube Refrigerator with Linear Compressor", *Cryocoolers 13*, p157-163

17. Lakeshore Cryotronics, Silicon Diode Installation Instructions, (2010)

18. www.cryogenics.nist.gov

19. Olson, J. R., Swift, G. W. (1999) "Suppression of Acoustic Streaming in Tapered Pulse Tubes", *Cryocoolers 10*, p307 - 313

20. Cha, J. S. et al. (2006) "Multi-dimensional flow effects in pulse tube refrigerators", *Cryogenics 46*, p658 – 665

Appendix A: Heater wire Thermal Loss Calculations

Input	Cold face temperature	77	K	
	Warm face temperature	300	K	
	Diameter	0.320685379	mm	
	Length	300	mm	
	conductivity	413	W/mk	
Thermal conduction calculations				
	Area	8.07696E-08	m^2	
	R	8993.3812		
	Heat flux	0.024796013	W	for 10W power
		0.099184053	x4 wires	W heat loss
	Material1/2 junction temp	300	K	
Electrical Resistance Calculations				
	k	0.000000017	ohm.meter	
	Resistance	0.049592027	W	
		0.099184053	x2 wires	W current loss
	Total power loss	0.198368107	W	

	W/mk
Teflon	0.26
copper	413
Constantan	23

Figure A.1. Thermal and electrical loss calculation to optimise wire diameter into cold space.

Appendix B: Pulse and Regenerator Tube Thermal Conduction Hand-Calculations

Axial conduction down the pulse tube

$k := 6\frac{W}{m \cdot K}$ Stainless steel 304 tubes

k varies with temperature, so this is an average value for k between 300 and 50 K.

$ODpt := 21.8mm$

$IDpt := 21mm$

$Apt := \left[(ODpt)^2 \cdot \frac{\pi}{4}\right] - \left[(IDpt)^2 \cdot \frac{\pi}{4}\right]$

$Apt = 2.689 \times 10^{-5} m^2$

$T1 := 300K$

$T2 := 50K$

$x1 := 70mm$

$H := k \cdot Apt \cdot \frac{(T1 - T2)}{x1}$

$H = 0.576W$

Axial conduction down the regenerator tube

$ODreg := 44.8mm$

$IDreg := 44.0mm$

$Areg := \left[(ODreg)^2 \cdot \frac{\pi}{4}\right] - \left[(IDreg)^2 \cdot \frac{\pi}{4}\right]$

$Areg = 5.579 \times 10^{-5} m^2$

$T1 := 300K$

$T2 := 50K$

$x2 := 44mm$

$H2 := k \cdot Areg \cdot \frac{(T1 - T2)}{x2}$ $k = 6\frac{m \cdot kg}{K \cdot s^3}$

$H2 = 1.902W$

A further calculation was carried out on the regenerator tube, using NIST values for the varying thermal coefficient k:

$a := -1.408$

$b := 1.398$

$c := 0.254$

$d := -0.626$

$e := 0.233$

$f := 0.425$

$g := -0.465$

$h := 0.165$

$i := -0.019$

$$nn(T) := a + b\cdot\log(T) + c\cdot(\log(T))^2 + d\cdot(\log(T))^3 + e\cdot(\log(T))^4 + f\cdot(\log(T))^5 + g\cdot(\log(T))^6 + h\cdot(\log(T))^7 + i\cdot(\log(T))^8$$

$$k(T) := 10^{(nn(T))}$$

$T := 30, 60.. 300$

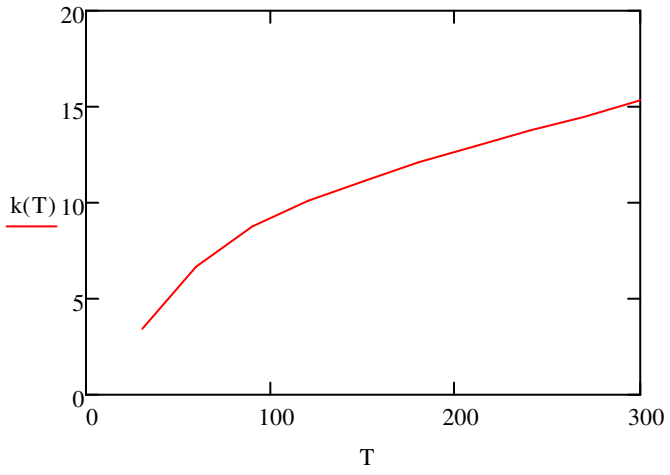

$$Q := \int_{50}^{300} k(T)\, dT$$ Thermal conductivity

$Q = 2.891\times 10^3 \quad \frac{W}{m}$

$$A := \frac{Areg}{m^2}$$

$$A = 5.579 \times 10^{-5}$$

$$x := 0.04$$

$$qdot := Q \cdot \frac{A}{x}$$

$$qdot = 3.666 \ W$$

The end condition conductivity could also affect result

Appendix C: Radiation Heat Leak Calculation

Worst case radiation leak into the cryostat:

$\sigma := 5.67 \times 10^{-8}$ Stefan Boltzman constant

$\varepsilon := 1$

$T := 300$

$A := 7.2 \cdot 10^{-3}$

$Power := \sigma \cdot A \cdot T^4 \cdot \varepsilon$

$Power = 3.307\ W$ Loss at the cold-head with 300K radiating onto cold-head with $\varepsilon = 1$
This is the very worst-case emmissivity

Appendix D: PT2050 Assembly Drawings

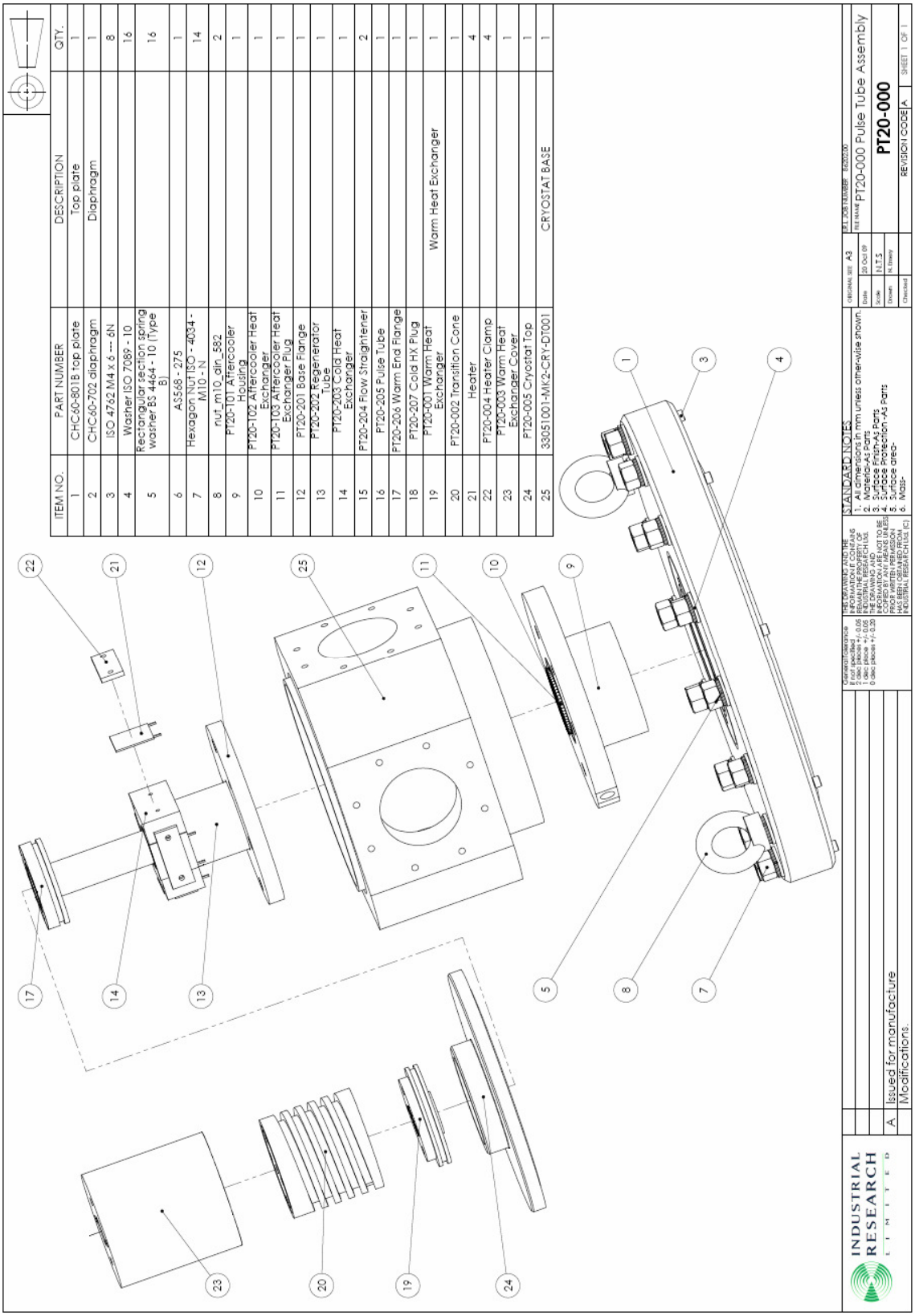

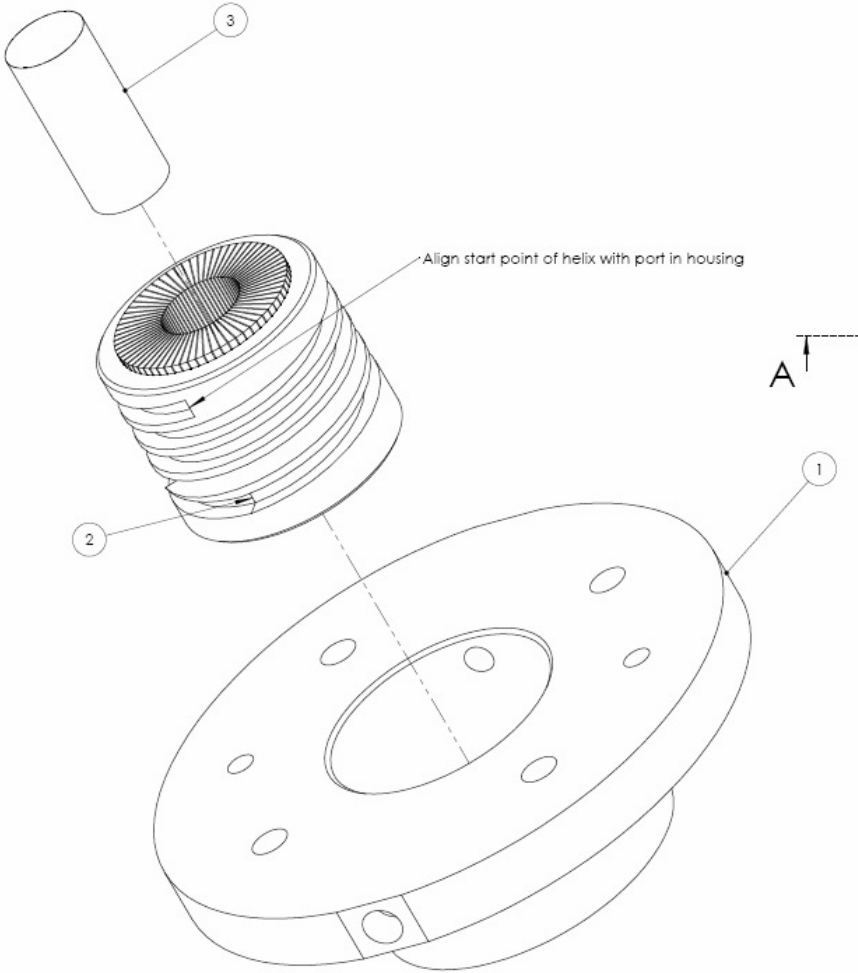

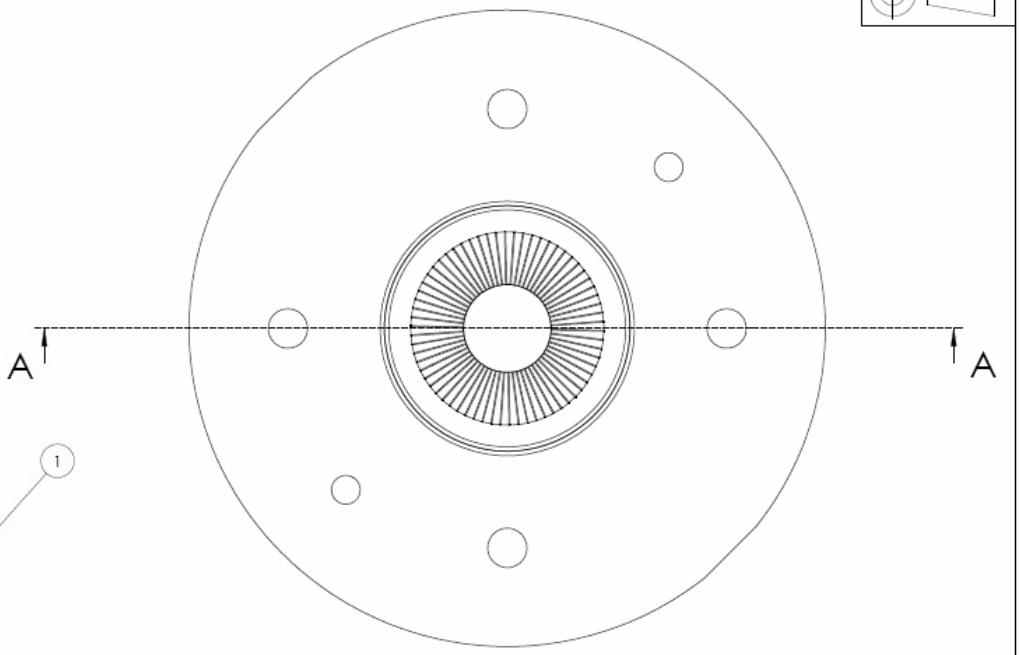

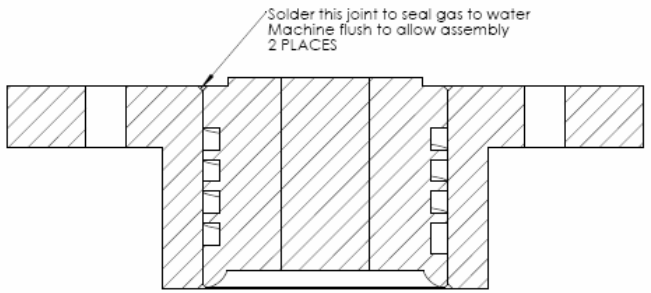

SECTION A-A
SCALE 1 : 1

ITEM NO.	PART NUMBER	DESCRIPTION	QTY.
1	PT20-101 Aftercooler Housing		1
2	PT20-102 Aftercooler Heat Exchanger		1
3	PT20-103 Aftercooler Heat Exchanger Plug		1

INDUSTRIAL RESEARCH LIMITED

A	Issued for manufacture
	Modifications.

General Tolerance
If not specified
2 dec places +/- 0.05
1 dec place +/- 0.05
0 dec places +/- 0.20

STANDARD NOTES
1. All dimensions in mm unless other-wise shown.
2. Material-As Parts
3. Surface Finish-As Parts
4. Surface Protection -As Parts
5. Surface area-
6. Mass-

ORIGINAL SIZE	A3
Date	20 Oct 09
Scale	N.T.S
Drawn	N. Emery
Checked	

IRL JOB NUMBER 84202.00
FILE NAME PT20-100 Aftercooler Assembly

PT20-100

REVISION CODE A | SHEET 1 OF 1